LLNL-JRNL-752477

Using eclogite retrogression to track the rapid exhumation of the Pliocene Papua New Guinea UHP Terrane

J. W. DesOrmeau, S. M. Gordon, T. A. Little, S. A. Bowring, B. Schoene, K. M. Samperton, A. R. C. Kylander-Clark

June 5, 2018

Journal of Petrology

Disclaimer

Using eclogite retrogression to track the rapid exhumation of the Pliocene Papua New Guinea UHP Terrane

Joel W. DesOrmeau[1]*, Stacia M. Gordon[1], Timothy A. Little[2], Samuel A. Bowring[3], Blair Schoene[4], Kyle M. Samperton[4,5], and Andrew R.C. Kylander-Clark[6]

[1]Department of Geological Sciences, University of Nevada Reno, Nevada, 89557 USA; [2]School of Geography, Environment and Earth Sciences, Victoria University of Wellington, Wellington, 6140 New Zealand; [3]Department of Earth, Atmospheric, and Planetary Sciences, Massachusetts Institute of Technology, Cambridge, Massachusetts, 02139 USA; [4]Department of Geosciences, Princeton University, Princeton, New Jersey, 08544 USA; [5]Nuclear and Chemical Sciences Division, Lawrence Livermore National Laboratory, Livermore, California, 94550 USA; [6]Department of Earth Science, University of California, Santa Barbara, California, 93106 USA

*Corresponding author. Telephone: 1-775-784-6054. Email: jdesormeau@unr.edu

Key words

CA-ID-TIMS-TEA; LASS; eclogite retrogression; zircon REE

ABSTRACT

The D'Entrecasteaux Islands of eastern Papua New Guinea (PNG) host the youngest known ultrahigh-pressure terrane on Earth and represent the only location where ultrahigh-pressure (UHP) rocks have been exhumed in an active rift. The PNG (U)HP rocks, consisting of Pliocene eclogites, garnet amphibolites, and migmatitic gneisses, are exposed in five domal structures across the Islands. Zirconium-in-rutile thermometry records peak temperatures of ~780 ºC from the eastern Oiatabu and nearby central Mailolo Domes, and hotter temperatures of ~825–865 ºC within the western Goodenough Dome. Uranium-lead (U-Pb) and trace-element zircon compositions from a suite of eclogite, host gneiss, felsic dikes, and pegmatite from three domes document the rapid exhumation history of the PNG UHP terrane. High-spatial resolution laser-ablation split-stream–inductively coupled plasma–mass spectrometry (LASS ICP-MS) analyses of select eclogite zircon exhibit no resolvable age zoning within single crystals. The same eclogite zircon, combined with separate zircon extracted from additional eclogite, host gneiss and felsic intrusions, were subsequently analyzed by high-precision U-Pb chemical-abrasion–isotope-dilution–thermal ionization mass spectrometry and solution ICP-MS trace-element analysis (TIMS-TEA). The results record discrete tectonic events across the three domes at sub-million year timescales: 1) (re)crystallization of host gneiss within the lower crust exposed in eastern Oiatabu Dome from ca. 5.7–4.5 Ma; 2) initial retrogression of eclogites from Oiatabu and Mailolo Domes at ca. 4.6–4.3 Ma; 3) melt crystallization of weakly deformed felsic dikes of Oiatabu Dome at ca. 3.0–2.9 Ma; and 4) retrogression and melt crystallization within eclogite–amphibolite-facies rocks in the western Goodenough Dome at ca. 2.9–2.6 Ma. In comparison to Zr-in-rutile peak temperature estimates, Ti-in-zircon temperatures >800 ºC may reflect increased temperatures during exhumation that resulted in partial melting of the eclogites. Inclusions of

crystallized hydrous melt consisting of Na-rich plagioclase ± K-feldspar + quartz within eclogite zircon document this process. The elevated temperatures and the presence of the polyphase inclusions are the first documentation of partial melting of the (U)HP eclogites within PNG during initial retrogression from ca. 4.6–4.3 Ma. Overall, U-Pb zircon geochronology and geochemistry track both the timing of retrogressive overprinting within the lower-to-middle crust and final upper crustal emplacement over a relatively short span of ~ 2 Myr during the rapid (≥ 2.3 cm/yr) exhumation of the youngest known (U)HP eclogites.

INTRODUCTION

The subduction of low-density continental lithosphere to mantle depths and its subsequent exhumation are widely recognized through the preservation of coesite and diamond within eclogites and, less commonly, host gneisses of Phanerozoic orogens (i.e. Chopin, 1984; Smith, 1984; Sobolev & Shatsky, 1990; Ernst et al., 2001; O'Brien, 2001; Liou et al., 2004; Hacker, 2007; Liu et al., 2007; Gilotti, 2013). Multiple geochronological techniques have been applied to phases within eclogite and host gneiss to determine the timing of peak UHP metamorphism (U-Pb zircon, monazite, and allanite; Lu–Hf and Sm–Nd garnet) and retrogressive overprinting at lower pressure eclogite–amphibolite-facies conditions (U-Pb titanite, rutile, and zircon; Sm-Nd garnet; Rb-Sr multimineral isochrons). These combined approaches track the temporal evolution of subducted continental lithosphere from the mantle to the upper crust by revealing various subduction–exhumation rates. In general, large (30,000 km^2), thick, and slow terranes record longer, ca. 10–30 Myr subduction–exhumation durations (e.g. Hacker et al., 2003, 2006; Kylander-Clark et al., 2007, 2009), whereas small (4,000 km^2), thin, and fast terranes were subducted and exhumed in <10 Myr (e.g. Gebauer et al., 1997; Amato et al., 1999; Rubatto &

Hermann, 2001; Lapen et al., 2003; Parrish et al., 2006; Kylander-Clark et al., 2012; Korchinski et al., 2014).

Multiple UHP terranes record fast exhumation rates (>1 cm/year) from mantle depths to the lower crust [Erzgebirge and Kokchetav: Hermann et al., 2001, Hacker et al., 2003, Massonne et al., 2007; Tso Morari: de Sigoyer et al., 2000; Dora Maira: Rubatto & Hermann, 2001; Kaghan Valley: Kaneko et al., 2003; Parrish et al., 2006; Papua New Guinea: Monteleone et al., 2007; Baldwin et al., 2008; Zirakparvar et al., 2011; DesOrmeau et al., 2017]. Fast initial exhumation rates have been attributed to buoyancy forces [i.e. large density contrast between the mantle and subducted material; e.g. Ernst et al., 1997] overcoming boundary tractions (e.g. Warren et al., 2008). For most UHP terranes, this portion of the exhumation to the base of the crust is characterized by near-isothermal decompression (e.g. Rubatto & Hermann, 2001; Parrish et al, 2006; Monteleone et al., 2007) accompanied by partial melting of host gneiss and possibly eclogite (e.g. Labrousse et al., 2011; Ganzhorn et al., 2014). The presence of melt weakens the exhuming body while simultaneously enhancing its buoyancy (e.g. Hill et al., 1995; Wallis et al., 2005; Lang & Gilotti, 2007; Gerya et al., 2008; Faccenda et al., 2009; Ragozin et al., 2009; Ellis et al., 2011; Labrousse et al., 2011; Li et al., 2011; Little et al., 2011; Gordon et al., 2012; Sizova et al., 2012).

Within eastern Papuan New Guinea (PNG) (Fig. 1), multiple domal structures expose Pliocene (U)HP rocks (Fig. 2; e.g. Davies & Warren, 1988, 1992; Hill & Baldwin, 1993; Baldwin et al., 2008; Little et al., 2011). Throughout the domes, the eclogites represent metamorphosed, disrupted mafic dikes that have been fractured and boudinaged into meter- to decameter-scale lenticular blocks within host migmatitic gneiss (Hill, 1994; Little et al., 2011). In addition, there is abundant evidence of partial melting in the form of layer-parallel leucosomes, dikes, and plutons (Hill et al., 1995; Gordon et al., 2012; Little et al., 2013; DesOrmeau et al., 2014).

The domes of eastern PNG represent an ideal locality to investigate rapid UHP exhumation and the influence of melt-assisted exhumation. Previous studies of this UHP terrane argue for a rapid (>1 cm/yr), near-isothermal decompression path, with the crustal rocks undergoing UHP metamorphism at ca. 7.9–5.2 Ma, melt crystallization from ca. 4.1–2.8 Ma, and exhumation to the near surface by ca. 1.8–0.3 Ma (Davies & Warren, 1988; Hill & Baldwin, 1993; Monteleone et al., 2007; Baldwin et al., 2008; Fitzgerald et al., 2008; Little et al., 2011; Zirakparvar et al., 2011; Gordon et al., 2012; DesOrmeau et al., 2014, 2017). In the present study, zircon U-Pb dates and trace-element compositions were obtained by single-grain, chemical abrasion–isotope dilution–thermal ionization mass spectrometry (CA-ID-TIMS; Mattinson, 2005) and solution inductively coupled plasma mass spectrometry (ICP-MS; TIMS-TEA of Schoene et al., 2010) from multiple variably-retrogressed eclogites, garnet amphibolite, host gneisses, and weakly deformed felsic dikes and pegmatite from three domes to more precisely document metamorphic, melt-crystallization, and deformational events during the exhumation of the UHP terrane. In addition, transects across individual eclogite zircon were analyzed by laser-ablation split-stream (LASS) ICP-MS prior to TIMS-TEA to investigate intra-crystal age and trace-element zoning. These results provide insight to the geodynamic processes involved in the subduction and rapid transfer of continental material through the lower crust to Earth's surface via coupled buoyancy-driven and extension-related exhumation processes.

GEOLOGIC SETTING

Woodlark Basin

Ongoing convergence of the Pacific and Australian plates at a rate of ~10–11 cm/yr has resulted in the formation and rotation of microplates near eastern PNG since the Eocene (Fig. 1; Tregoning et al., 1998; Wallace et al., 2004, 2014). During the Paleogene, this convergence caused the Papuan Orogen collisional event, which resulted in northeast-oriented subduction of the northern Australian rifted margin beneath an island-arc terrane (Davies & Jacques, 1984; Cloos et al., 2005; Little et al., 2011). The island-arc basement [Papuan Ultramafic Belt (PUB)] was obducted along the Owen Stanley Fault on the mainland Papuan Peninsula during this event (Lus et al., 2004). Subduction continued until the early Miocene (Davies & Jacques, 1984; Rogerson et al., 1987; Davies, 1990; Davies & Williamson, 1998; Van Ufford & Cloos, 2005; Davies, 2012). Some Australian-plate rocks were subducted to mantle depths likely during the Paleogene to early Miocene; this continental material is interpreted as the protolith for the UHP terrane exposed in the D'Entrecasteaux Islands (Fig. 1; Zirakparvar et al., 2013).

In the late Miocene, plate reorganization related to continued oblique convergence between the Pacific and Australian plates caused the initiation of north-northwestward subduction of the Solomon Sea microplate at the New Britain Trench (Fig. 1; Weissel et al., 1982; Wallace et al., 2004, 2014). Slab pull associated with this subduction has caused counterclockwise rotation of the Woodlark and Solomon Sea microplates relative to Australia since the late Miocene (Fig. 1; Wallace et al., 2004, 2014; Webb et al., 2008; Cairns et al., 2015). Since 6 Ma, this rotation has been accommodated by seafloor spreading within the Woodlark Basin and continental rifting within the Woodlark Rift (Fig. 1; Taylor et al, 1999; Kington & Goodliffe, 2008). The D'Entrecasteaux Islands are positioned in the center of this rift, with rifting-associated extension having resulted in the formation of a series of 2.0–2.5 km-high gneiss domes (Figs 1 and 2; Davies & Warren, 1988). Combined geophysical, geodetic, and structural results suggest significant thinning at all levels of the lithosphere, from apparent removal of the mantle lithosphere, to vertical thinning of the crust, which has thinned from ~30–50 km to ~20 km beneath the domes (Tregoning, 1998; Taylor et al., 1999; Abers 2001; Abers et al., 2002; Wallace et al., 2004, 2014; Little et al., 2011, 2013; Eilon et al., 2014, 2015).

D'Entrecasteaux Islands

The D'Entrecasteaux Islands host five gneiss domes: Normanby (northwest Normanby Island), Morima (southern Fergusson Island), Oiatabu (eastern Fergusson Island), Mailolo (western Fergusson Island), and Goodenough (Goodenough Island; Fig. 2). The lower plates of the domes consist mainly of migmatitic quartzofeldspathic orthogneiss, with lesser amounts of eclogite and amphibolite, marble, paragneiss, and quartzite (Davies & Warren, 1988, 1992; Hill et al., 1992; Baldwin et al., 2004, 2008; Monteleone et al., 2007; Little et al., 2011, 2013). Minor remnants of the PUB and its nonmetamorphosed Neogene volcanic and sedimentary cover are exposed in the upper plate of the domes (Fig. 2; Davies & Warren, 1988). Active 30–40° dipping normal faults flank the northern margins of Oiatabu, Mailolo, and Goodenough Domes and the southwestern margin of the Morima Dome. Little et al. (2011) show that these faults cut an older, more gently dipping structural boundary, the D'Entrecasteaux fault zone (Fig. 2), which is interpreted to be correlative to the Owen Stanley Fault (Fig. 1).

The lower plates can be structurally divided into an uppermost carapace zone (up to 1.5 km thick) that shows a strong, planar LS tectonite fabric, and an inner, structurally deeper, core zone with more chaotic fabrics (Fig. 2; Hill, 1994). Eclogite–amphibolite-facies mafic rocks, layer-parallel leucosomes, dikes, and plutons, and evidence for melt-present deformation are evident throughout all structural levels of the domes (Little et al., 2011, 2013); however, the amount of leucosome increases from ~15 vol. % in the carapace to upwards of 70 vol. % in the dome cores (Gordon et al., 2012).

Previous thermobarometry studies of UHP eclogites from the D'Entrecasteaux Islands

Only eclogites from the Oiatabu, Mailolo, Morima, and Goodenough Domes have been targeted for pressure–temperature (*P–T*) investigation. Coesite has only been identified thus far in one Mailolo Dome eclogite (Baldwin et al., 2008). Detailed cation-exchange thermobarometry, *P–T* pseudosection modeling, and Zr-in-rutile thermometry of an eclogite from this same coesite-bearing outcrop yield estimates of UHP conditions at ~27–31 kbar and ~715 ºC (DesOrmeau et al., 2017). Cation-exchange thermobarometry of other eclogites from the four domes have yielded results ranging from 12–24 kbar and 530–840 ºC (Davies & Warren, 1992) and 20–24 kbar and 730–930 ºC (Hill & Baldwin, 1993; Baldwin et al., 2004). The considerable range in *P–T* from these domes may reflect different subduction–exhumation histories experienced by the domes. Alternatively, uncertainty in clinopyroxene Fe^{3+} content for the garnet-clinopyroxene thermometer may also influence these variable results (i.e. Proyer et al., 2004).

Previous geochronological studies of the D'Entrecasteaux Islands

Efforts to determine the timing and duration of PNG (U)HP metamorphism have utilized several different isotopic systems, including Lu-Hf garnet–whole rock isochrons, U-Pb zircon, $^{40}Ar/^{39}Ar$ phengite, and Rb-Sr whole rock–omphacite–phengite isochrons; these previous studies have focused on eclogites from the Mailolo and Goodenough Domes only. The coesite-eclogite from Mailolo Dome yielded variable results ranging from ca. 8–5 Ma [SIMS U-Pb zircon, Monteleone et al., 2007; Lu-Hf garnet–whole rock, Zirakparvar et al., 2011; CA-ID-TIMS U-Pb zircon, Gordon et al., 2012; $^{40}Ar/^{39}Ar$ phengite, Baldwin & Das, 2015]. Zircon separates containing inclusions of the well-equilibrated peak mineral assemblage yield individual CA-ID-TIMS $^{206}Pb/^{238}U$ (Th-corrected) dates of 6.0 ± 0.2 to 5.2 ± 0.3 Ma (2σ uncertainty unless otherwise stated). These inclusions were identical in composition to matrix phases used in determining the UHP *P–T* estimates discussed above suggesting that these dates are a reliable estimate for the timing of UHP metamorphism (DesOrmeau et al., 2017).

Additional zircon SIMS analyses from other eclogites have resulted in $^{206}Pb/^{238}U$–$^{207}Pb/^{206}Pb$ Terra–Wasserburg intercept dates ranging from 4.3 ± 0.4 Ma (MSWD = 3.3) in Mailolo Dome (Baldwin et al., 2004) to 2.9 ± 0.4 (MSWD = 1.02) to 2.1 ± 0.5 Ma (MSWD = 4.2) in Goodenough Dome (Monteleone et al., 2007). A Rb-Sr whole-rock–omphacite–phengite isochron date of 5.6 ± 1.6 Ma (MSWD = 1.0) was also previously obtained for an eclogite from Mailolo Dome (Korchinski et al., 2014).

Throughout all the domes, CA-ID-TIMS geochronology of variably deformed crystallized melt (leucosomes, sills, dikes, and plutons) records the exhumation of the (U)HP rocks and dome formation. Zircon CA-ID-TIMS dates from a variety of strongly deformed sills and layer-parallel leucosomes suggest that the (U)HP rocks were exhumed to lower-crustal levels by ca. 4.1 Ma in the eastern Normanby Dome (DesOrmeau et al., 2014), by ca. 3.5–3.0 Ma to the west in Mailolo Dome (Gordon et al., 2012), and in the far west Goodenough dome by ca. 3.9–2.8 Ma (DesOrmeau et al., 2014). Strongly-deformed host gneiss from Mailolo dome records U-Pb zircon SIMS depth profiling dates of 3.66 ± 0.13 Ma (MSWD = 1.6) that are slightly older than the layer-parallel leucosomes (Zirakparvar et al., 2014). Weakly-deformed felsic dikes likely record late-stage ponding and ductile deformation during amphibolite-facies retrogression of the domes at ca. 2.4 Ma within Mailolo Dome (Gordon et al., 2012) and ca. 2.3 Ma in Goodenough

Dome (DesOrmeau et al., 2014). Termination of ductile deformation and final dome emplacement are recorded by the crystallization of non-deformed dikes and plutons that cross-cut the dome-defining foliation throughout all the D'Entrecasteaux domes by ca. 1.8 Ma (Baldwin et al., 1993; Gordon et al., 2012; DesOrmeau et al., 2014).

Thermochronology provides further estimates on the cooling history of the domes between ~500–80 ºC. Mailolo Dome gneiss and pegmatite yielded $^{40}Ar/^{39}Ar$ hornblende, white mica, and biotite dates of ca. 3.5–2.6 Ma, whereas Goodenough Dome gneiss produced a range of dates from ca. 3.0–1.5 Ma (Baldwin et al., 1993; Waggoner et al., 2008). Apatite (U-Th)/He and fission-track ages record the final emplacement of the domes within the shallow crust by ca. 1.8–0.3 Ma (Fitzgerald et al., 2008).

Preservation of PNG (U)HP eclogites

The degree to which the mafic boudins preserve (U)HP assemblages is variable across the domes. Peak eclogite-facies assemblages in Mailolo Dome eclogites are typically well-preserved. This inference is based on: 1) the presence of coesite (Baldwin et al., 2008); 2) Jadeite-rich omphacite (>Jd_{60}); and 3) high silica content of phengite (up to Si = 3.5 atoms/per formula unit; Davies & Warren, 1992; Hill & Baldwin, 1993; Baldwin et al., 2004, 2008; DesOrmeau et al., 2017). Approximately 10 km to the east, Oiatabu Dome also contains a kyanite–phengite (up to Si = 3.5 apfu) eclogite that may have experienced UHP conditions, although coesite has not yet been found. In addition, omphacite in this eclogite and another kyanite-bearing eclogite has lower Jd contents ($Jd_{28–32}$; DesOrmeau, 2016). In comparison, to the west, Goodenough Dome mafic assemblages consist of diopsidic clinopyroxene ($Jd_{0–12}$), no omphacite, and a typical matrix of garnet, amphibole, plagioclase, and biotite (Davies & Warren, 1992; Monteleone et al., 2007; DesOrmeau, 2016).

(U)HP ECLOGITES, GARNET AMPHIBOLITE, GNEISSES, AND DIKES SAMPLED ACROSS THE D'ENTRECASTEAUX ISLANDS

This study applies high-precision CA-ID-TIMS zircon geochronology to a suite of eclogites from three of the domes to refine the temporal history of exhumation and associated amphibolite-facies retrogression given the rapid progression of tectonic events in PNG. Samples of host gneiss and dikes were also analyzed by CA-ID-TIMS to better understand the timing of host-rock metamorphism and the final stages of melt crystallization and deformation during emplacement within the upper crust for the less well-studied Oiatabu Dome. Finally, a pegmatite in close spatial association with a garnet amphibolite collected within the Goodenough Dome was analyzed to compare the timing of retrogression with pegmatite crystallization. Most samples were collected *in situ*; however, of the five mafic samples, three were collected as cobbles in creeks. The samples likely originated from the structural level from which they were collected given the steep topography and the exposures of the different structural levels across the domes (i.e. Oiatabu Dome exposes the carapace only; Fig. 2). Mailolo and Goodenough eclogite cobbles (PNG09-039b, PNG12-82a) were collected from drainages within their respective core zones and could have been sourced from exposures upstream within either the core or carapace zone (Fig. 2).

Oiatabu Dome (Fergusson Island)

One eclogite, three host gneisses, and two felsic dike samples were collected in the carapace zone of the eastern Oiatabu Dome. An eclogite cobble (PNG12-95a) was collected ~2 km from the eastern dome-bounding fault along the Basuenoia River and is the first eclogite to be dated from Oiatabu Dome (Fig. 2). The eclogite consists of anhedral–subhedral garnet (≤ 1.0 cm diameter) within a matrix of omphacite, coarser light green euhedral amphibole (≤ 1.0 cm), symplectite of clinopyroxene and plagioclase, and quartz with lesser rutile, apatite, and epidote (Figs 3a and b). Coarse amphibole and kelyphitic amphibole replace garnet, whereas replacement of omphacite by fine-grained symplectite of less Na-rich clinopyroxene and plagioclase is pervasive. Omphacite is found with garnet, quartz, apatite, and rutile (Fig. 3b). Minor coarse rutile (≤ 0.30 cm) occurs as a matrix phase associated with quartz, garnet, omphacite, amphibole, and fine-grained symplectite. The eclogite-facies assemblage was Grt + Omp + Qz + Rt ± Amp ± Lws [assumed precursor to epidote; mineral abbreviations after Whitney & Evans, 2010]. Fresh Grt + Omp + Ky ± Ph eclogite samples collected from the southwest corner of Oiatabu Dome and originally studied by Davies & Warren (1992) did not yield zircon.

Five samples of strongly-deformed host gneiss and younger felsic dikes were collected near the Basuenoia River eclogite. A migmatitic muscovite-bearing host paragneiss (PNG12-85a) was sampled from close to the eastern dome-bounding fault (Fig. 2). The remaining samples were collected ~1 km farther west and structurally deeper but still within the dome carapace. Host orthogneiss PNG12-87a contains dominantly quartz and feldspar with lesser biotite, whereas nearby orthogneiss PNG12-92a contains abundant biotite with minor quartz and plagioclase. Weakly-deformed quartzofeldspathic dikes (PNG12-87b and PNG12-92b) that cut the host gneisses from the same outcrop were also collected.

Mailolo Dome (Fergusson Island)

Two eclogite samples were collected from the core zone of Mailolo Dome along the Fagululu River within western Fergusson Island (Fig. 2). Sample PNG09-041c was collected *in situ* and is a medium- to coarse-grained eclogite consisting of garnet and omphacite within a matrix of amphibole and symplectite of clinopyroxene and plagioclase. Partial breakdown of the subhedral–euhedral garnet (0.5–1.0 cm) is marked by thin rims of retrograde amphibole and plagioclase (Fig. 3c). Garnet cores contain inclusions of early amphibole, whereas some rims contain rutile, zircon, omphacite, and apatite. In comparison, omphacite contains mostly rutile inclusions. Amphibole and a clinopyroxene–plagioclase symplectite replace omphacite rims and occasionally cores. Interstitial coarse apatite occurs with garnet, amphibole, plagioclase, and rutile. Coarse (re)crystallized zircon (~200 μm) are found throughout the entire thin section and are completely-to-partially enclosed by retrograde amphibole along garnet rims (Fig. 3c), coarse matrix amphibole, relict omphacite, symplectite of clinopyroxene and plagioclase, calcite–dolomite, and the assemblage rutile, apatite, and quartz. Rutile occurs as inclusions within garnet and as matrix grains associated with partially broken-down omphacite + garnet, coarse apatite, calcite–dolomite, and amphibole + plagioclase. The peak eclogite-facies assemblage was Grt+ Omp + Rt + Ap + Qtz (± Ph).

Along the same drainage within the core zone, eclogite PNG09-039b was collected as a cobble and is composed of coarse garnet (≤ 1.0 cm) and omphacite set in a matrix of phengite, biotite, dolomite, minor kyanite and allanite, and fine-grained symplectite along the margins of garnet, omphacite, and phengite. Like the matrix zircon from eclogite PNG09-041c, rounded (~200 μm) zircon, rutile, apatite, and quartz are found along garnet rims and within the matrix symplectite of clinopyroxene, plagioclase, and amphibole (Fig. 3d). Garnet is rimmed by amphibole, and small zircon (10–30 μm), rutile, and apatite occur with the amphibole and as inclusions within garnet. The peak eclogite-facies assemblage was Grt + Omp + Ph + Rt + Qtz ± Ap.

Goodenough Dome (Goodenough Island)

An eclogite and a garnet amphibolite were collected from the core zone along the Galuwata and Fakwaoia Rivers on the northern and southern flanks of Goodenough Dome, respectively (Fig. 2). An outcrop along the Galuwata River exposes discordant granitic pegmatite (PNG10-035b) that locally intrudes into a large garnet-amphibolite body, isolating numerous mafic pieces within the pegmatite; sample PNG10-035a is a piece of this garnet amphibolite. In comparison, eclogite PNG12-82a was collected as a stream cobble ~10 km to the southwest (Fig. 2).

Garnet amphibolite PNG10-035a is medium to coarse grained with euhedral–anhedral garnet (≤ 0.5 cm) set in a matrix of amphibole, plagioclase, Na-poor clinopyroxene, quartz, and biotite (DesOrmeau, 2016). Garnet inclusions consist of clinopyroxene, amphibole, and plagioclase, and kelyphitic amphibole growth replaces garnet rims (Fig. 3e). Some curvilinear grain boundaries between garnet, amphibole, and plagioclase progress towards garnet cores suggesting the abundant secondary amphibole and plagioclase grew partly at the expense of primary garnet. In addition, smaller fragments of garnet (0.05–0.5 cm) are mainly enclosed by plagioclase and quartz. Coarse amphibole typically contains plagioclase inclusions, and fine intergrowths of plagioclase and quartz are found in a clinopyroxene lath (≤ 0.3 cm in length). Rutile is included within garnet, amphibole, and plagioclase and is found along grain boundaries with matrix clinopyroxene, plagioclase, and amphibole. The HP assemblage was Grt + Cpx + Amp + Qz + Bt + Rt.

Eclogite PNG12-82a is composed of abundant subhedral to anhedral garnet within a matrix of amphibole, plagioclase, and lesser Na-poor clinopyroxene, biotite, and quartz. Inclusions of clinopyroxene within garnet are more Na-rich compared to matrix clinopyroxene (DesOrmeau, 2016). Breakdown of peak phases is pervasive, with symplectite of clinopyroxene and plagioclase present along garnet margins and cracks and, replacement of clinopyroxene by amphibole and plagioclase. Accessory zircon occurs within matrix amphibole (Fig. 3f). Rutile occurs as a matrix phase with biotite, amphibole, and plagioclase. The HP assemblage was Grt + Cpx ± Omp + Qz + Bt + Rt.

In summary, while all the mafic samples studied here show some degrees of retrogression (in comparison to the Mailolo coesite eclogite), we interpret that the Mailolo eclogites PNG09-039b and PNG09-041c and Oiatabu eclogite PNG12-95a equilibrated at higher *P–T* conditions and/or are less retrogressed in comparison to the Goodenough eclogite PNG12-82a and garnet amphibolite PNG10-035a samples.

METHODS

Zircon was extracted from the eclogites, the garnet amphibolite, the Oiatabu Dome gneisses and dikes, and the Goodenough Dome pegmatite via standard mineral separation techniques. A combination of single grains, microsampled fragments of grains, and multiple fragments of the same grain were analyzed by high-precision U-Pb zircon chemical abrasion TIMS-TEA (Schoene et al., 2010). Chemical abrasion removes high-U zircon domains susceptible to Pb-loss, thereby largely mitigating Pb-loss and the generation of anomalously young U-Pb dates (Mattinson, 2005). TIMS-TEA allows for the same zircon, or fragment of zircon, dated by ID-TIMS to be analyzed for trace-element composition (e.g. Schoene et al., 2010).

Prior to TIMS-TEA analysis, all grains were annealed at 900 ºC for 60 h and chemically abraded at 220 ºC for 12 h (Mattinson, 2005; see online supplement for further details). An unavoidable analytical challenge in dating Pliocene zircon with any technique (i.e. SIMS, LASS, ID-TIMS) arises from the low abundance of total ingrown radiogenic Pb, or Pb*, in many grains (typically Pb*<0.5 pg), and in all samples the especially low abundance of ^{207}Pb*. As such, ID-TIMS analyses of Pliocene zircons have a wide range of uncertainties for Th-corrected ^{206}Pb/^{238}U dates, which are inversely proportional to the radiogenic-to-common Pb ratio (Pb*/Pbc). Samples with especially low Pb* (≤ 1.0 pg) have much higher uncertainties on individual analyses, ranging from 1–8%, whereas those with high amounts of radiogenic Pb* (≥ 1.0 pg) have uncertainties ranging from 0.12–0.75% (Table SM1). Where applicable, reported ID-TIMS weighted-mean Th-corrected ^{206}Pb/^{238}U dates were calculated using the program ET_Redux (Bowring et al., 2011; McLean et al., 2011; Condon et al., 2015; McLean et al., 2015); otherwise all analyses throughout the text that do not define a single population are reported as individual Th-corrected ^{206}Pb/^{238}U dates. Uncertainties throughout the text, tables, and figures are at the 2σ or 95% confidence level. See figures 4, 5, SM1, and SM2, and Tables SM1 and SM3.

Zircon from most of the samples reveal a single TIMS age population (i.e. there are no obviously much younger zircon within a given sample), suggesting that inherited cores are not common within the whole grain or fragments of grains. However, to further assess intragrain temporal and compositional heterogeneity, representative zircon was mounted from four of the five mafic rocks, polished halfway through the grain, and imaged by cathodoluminescence (CL; Figs 4, 6 and 7). If inclusions were found within zircon, EDS analysis was used to identify the phases and their general composition.

After CL imaging, the grains were analyzed by LASS ICP-MS, which allows for the simultaneous collection of U-Th-Pb and trace-element data from an individual spot analysis (e.g. Kylander-Clark et al., 2013; see online supplement for detailed methodology). The LASS ICP-MS analyses consisted of transects and multiple spot analyses across grains to try to analyze all potential chemical/growth “zones” and trace-element heterogeneity within an individual grain. The four eclogite and garnet amphibolite samples analyzed by LASS ICP-MS contain the most radiogenic (Pb*) zircon of the mafic samples analyzed; thus, preparing a grain mount and polishing halfway through the grain did not drastically affect later ID-TIMS analyses of these same crystals. Zircon from the other eclogite (PNG12-82a), the three gneiss samples, dikes, and pegmatite was not polished and analyzed by LASS ICP-MS due to low Pb*. The LASS ICP-MS $^{206}Pb/^{238}U$ dates have typical uncertainties ranging from 2–11% for single-spot analyses, including both analytical and propagated uncertainties (Table SM2). The large uncertainties associated with some LASS ICP-MS measurements reflect the inherent difficulty in measuring such low amounts of radiogenic Pb*, given the small volume of ablated material. LASS ICP-MS analyses are reported as single-spot $^{206}Pb/^{238}U$ dates in figures 4, 6, SM1, and SM2 and tables SM2 and SM5.

Trace-element thermometry, including Ti-in-zircon (measured by laser ablation in grain mounts) and Zr-in-rutile (measured by electron-microprobe analysis in thin sections), was applied to the mafic samples to estimate the temperatures at which the zircon crystallized and the peak temperatures, respectively (Tables SM7 and SM8; see online supplement for detailed methodology). Ti-in-zircon temperatures were calculated using the calibration of Ferry & Watson (2007) assuming an activity of 1 for SiO_2 and TiO_2 based on the presence of quartz and rutile in all samples. Zr-in-rutile temperatures were calculated using the calibration of Tomkins et al. (2007) for the ß-quartz field with pressure estimates for each dome from previous *P–T* studies (Figs 8 and 9; Tables SM7 and SM8). We assumed pressures of 28 kbar for the Fergusson Domes and 16 kbar for Goodenough Dome for rutile thermometry based on the peak pressures attained by the coesite eclogite from the Fergusson Dome (Baldwin et al., 2008; DesOrmeau et al., 2017) and peak pressure estimates for the Goodenough Dome (Davies & Warren, 1992). For the Goodenough samples, the pressure estimate is taken as conservative and may underestimate the *P–T* conditions experienced by rocks across the dome. Analytical uncertainties for individual Ti-in-zircon and Zr-in-rutile estimates are ± 10–100 ºC and ± 10–25 ºC, respectively (Tables SM7 and SM8). Kernel density estimate plots for Zr-in-rutile and Ti-in-zircon temperatures are given for all samples in figure 9.

Garnet, plagioclase, and additional zircon trace-element data were collected in separate LA-ICP-MS analytical sessions for select mafic samples. These analyses were completed to better interpret the trace-element results from the zircon separated from the bulk rock (Tables SM5 and SM9). In addition, whole-rock compositional data for select mafic samples were performed by Activation Laboratories, Canada (Fig. 10; Table SM10); all trace-element analyses are normalized to chondrite values of McDonough & Sun (1995).

RESULTS

Zircon textures

Cathodoluminescence images of zircon extracted from the Oiatabu Dome eclogite PNG12-95a show large (~200–450 μm), euhedral, stubby, and angular grains that reveal sector zoning that either transitions smoothly to, or is truncated by, weak oscillatory zoning along the inner portions of the grain and the rims (Figs 4a, 6a and 7a). Some grains show a hazy, amorphous texture among weak sector and oscillatory zoning, while other grains have little to no zoning. Eclogites from Mailolo Dome, PNG09-041c and PNG09-039b, contain anhedral to rounded (40–300 μm) zircon that exhibit sector, oscillatory, and minor polygonal zoning. Zircon from PNG09-041c generally display weak zoning compared to more pronounced oscillatory and sector zoning in PNG09-039b (Figs 4b, c, 6b, c, 7b and c). Rare cores have been identified in PNG09-041c zircon (Figs 6b and 7b; Table SM2). Goodenough Dome eclogite PNG12-82a and garnet amphibolite PNG10-035a contain similar anhedral to rounded (40–300 μm) zircon that also typically show weak patchy- and polygonal-sector zones with some oscillatory zoning near the rims (Figs 4d, e, 6d and 7d). In comparison, host gneiss and dike samples contain euhedral prismatic grains with convolute zoning (~50–100 μm; Fig. 5).

Imaging revealed that many of the zircon from the mafic samples contain inclusions. Zircon from several samples contain polyphase inclusions with negative crystal shapes up to ~150 μm in diameter that vary in composition. Zircon recovered from heavy mineral separates of PNG12-95a contain polyphase inclusions of Ab + Qz (Fig. 7) and embayments of amphibole. For sample PNG09-041c, both *in situ* zircon that occurs with retrograde amphibole and plagioclase along garnet and omphacite boundaries and grains within polished mounts contain polyphase inclusions of Ksp + Qz + Ab ± Ap and individual inclusions of calcite–dolomite (Fig. 7). Sample PNG09-039b has similar polyphase inclusions, with Ksp + Qz + Ab ± Rt. Finally, mineral separate zircons from PNG10-035a contain polyphase inclusions of Rt + Pl + Bt + Chl and individual inclusions of garnet and calcite (Fig. 7).

U-Pb CA-ID-TIMS and LASS geochronology

Oiatabu Dome eclogite, host-gneiss, and dikes

Eclogite sample PNG12-95a is from the carapace of eastern Oiatabu Dome (Fig. 2). LASS transects across nine pink, very coarse [up to 450 μm in length; Figs 4a and 6a] prismatic zircon gave similar dates ranging from 4.70 ± 0.10 Ma to 4.44 ± 0.11 Ma (Fig. 4a; Table SM2), suggesting no discernible age zoning within the limits that can be resolved (<0.15 Myr) by the LASS method. CA-ID-TIMS whole-grain analyses fall within a narrow range from 4.63 ± 0.03 Ma to 4.58 ± 0.01 Ma (n = 16), including two of the same grains that were analyzed by LASS (Fig. 4a; Tables SM1 and SM2). In addition, to test for dispersion of CA-ID-TIMS dates within a single grain, a ~300 μm zircon was microsampled. The three fractions yield indistinguishable dates of 4.61 ± 0.03 Ma, 4.62 ± 0.01 Ma, and 4.62 ± 0.01 Ma (z16 in Fig. 4a; Table SM1).

Zircon from a host paragneiss sampled from the carapace of Oiatabu Dome (PNG12-85a) is prismatic and displays core and rim textures with convolute rim zoning (Fig. 5; Corfu et al., 2003). Zircon occurs within quartz and plagioclase ribbons and as inclusions within muscovite. Whole-grain CA-ID-TIMS analyses yield dates from 27.20 ± 0.06 Ma to 5.52 ± 0.04 Ma (n = 14; Table SM3). Analysis of only the microsampled zircon rim overgrowths give CA-ID-TIMS dates of 5.66 ± 0.05 Ma to 4.49 ± 0.04 Ma (n = 5; Fig. 5; Table SM3). Structurally deeper within the dome, another host gneiss, orthogneiss PNG12-87a, yields inherited whole-grain results from ca. 84–53 Ma (Table SM3). In comparison, zircon from a cross-cutting weakly deformed quartzofeldspathic dike (PNG12-87b) within the same outcrop give CA-ID-TIMS dates ranging 3.02 ± 0.06 Ma to 2.93 ± 0.01 Ma (n=7; Fig. 5; Table SM3). At similar structural levels and ~0.5 km to the south within the dome, a biotite-rich quartzofeldspathic orthogneiss (PNG12-92a) also only yields inherited whole-grain results from ca. 90–56 Ma (Table SM3). At the same outcrop, a weakly deformed cross-cutting pegmatitic quartzofeldspathic dike (PNG12-92b) yields zircon with dates that range from 5.56 ± 0.23 Ma to 2.97 ± 0.08 Ma (n=7; Fig. 5), and a single zircon gives an older date of ca. 89 Ma (Table SM3).

Mailolo Dome eclogites

Eclogite PNG09-041c contains abundant, large, ~100–300 μm, rounded matrix zircon (Fig. 3c). In addition, zircon is included within garnet. Thirty-one zircon analyzed by LASS give dates ranging from 5.54 ± 0.33 Ma to 4.33 ± 0.37 Ma (n = 42; Figs 4b and 6b), with a single analysis yielding an older discordant date of ca. 36 Ma (Fig. 6b; Table SM2). CA-ID-TIMS analyses yield dates of 4.65 ± 0.06 Ma to 4.51 ± 0.35 Ma (n = 12; Fig. 4b), with a weighted-mean $^{206}Pb/^{238}U$ date of 4.63 ± 0.01 Ma (MSWD = 0.70; n = 12). A single zircon analysis yields an older date of 5.41 ± 0.11 Ma (Table SM1).

Eclogite PNG09-039b also contains coarse (100–300 μm), rounded zircon and LASS analyses of twenty-nine zircon yields dates ranging from 4.82 ± 0.19 Ma to 4.10 ± 0.15 Ma (n = 49; Figs 4c and 6c; Table SM2). Subsequent CA-ID-TIMS analyses of seven of the same whole grains, or fragments of grains, give dates ranging from 4.38 ± 0.04 Ma to 4.33 ± 0.02 Ma (n = 10; Fig. 4c, Table SM1). Additional whole-grain analyses yield CA-ID-TIMS dates that cluster between 4.36 ± 0.08 Ma to 4.30 ± 0.02 Ma (n = 8; Fig. 4c; Table SM1).

Goodenough Dome garnet amphibolite and eclogite

For garnet amphibolite PNG10-035a, LASS analyses across three, large (100–200 μm), subhedral zircon give dates ranging from 3.46 ± 0.33 Ma to 2.81 ± 0.08 Ma (n = 6; Figs 4d and 6d; Table SM2), whereas CA-ID-TIMS analyses of the same grain fragments yield dates of 2.89 ± 0.03 Ma to 2.83 ± 0.23 Ma (n = 4; Fig. 4d; Table SM1). Additional CA-ID-TIMS analyses of whole grains give dates of 2.87 ± 0.08 Ma to 2.65 ± 0.03 Ma (n = 9; Fig. 4d; Table SM1). Zircon from the pegmatite that intruded the garnet amphibolite (PNG10-035b) give single-grain dates of 2.64 ± 0.09 Ma to 2.48 ± 0.02 Ma (n = 10; Fig. 5; Table SM3).

A zircon was identified within matrix amphibole of the retrogressed eclogite PNG12-82a (Fig. 4e). Zircon was only analyzed for U-Pb by CA-ID-TIMS due to the low amounts of radiogenic Pb (0.13–0.80 pg). Ten zircon yield dates of 2.78 ± 0.04 Ma to 2.62 ± 0.06 Ma (Fig. 4e; Table SM1).

Mineral and whole-rock chemistry and Ti-in-zircon and Zr-in-rutile thermometry

For all samples, zircon trace element results from solution ICP-MS, LASS, and LA-ICP-MS analyses (referred to as *in situ* trace-element analyses) are described together, as they give similar results. For most samples, *in situ* trace-element analyses show more variability in comparison to TEA results likely due to averaging of the much larger sample volume (whole-grain or fragment) analyzed with solution ICP-MS. There are no resolvable temporal trends with zircon composition or CL zoning observed in any sample. Reported Th/U ratios were directly measured with LASS, whereas the TEA results are the calculated model Th/U ratio from the CA-ID-TIMS analyses.

Oiatabu Dome eclogite

Zircon from Oiatabu Dome eclogite PNG12-95a reveals mostly absent Eu anomalies (Eu/Eu* = 0.66–1.15) (Figs 6a, SM1 and SM2; Tables SM4 and SM5) and depleted HREE patterns ($Lu_N/Gd_N < 2$), except for a single *in situ* analysis of $Lu_N/Gd_N = 5$ (Figs 6a, SM1, and SM2). Most analyses yield Th/U ratios between 0.39–1.00, but overall they range from 0.01–1.00 (Fig.

SM1; Tables SM4 and SM5). *In situ* analyses of the coarse zircon show a considerable spread in Ti concentrations from 2–115 ppm (Tables SM5 and SM7) resulting in temperatures of 620–1040 ºC (Figs 6a, 8 and 9b). Of these analyses, ten separate zircon record calculated Ti-in-zircon temperatures ≥ 850 ºC (n=13), and a transect across one grain (z3; n=7) details drastic variations (~300 ºC) and very high temperatures (up to 1000 ºC) (Figs 6a, 8 and 9b). *In situ* analyses with lower Ti values (~<9 ppm) correspond to lower REE abundances and Th/U ratios; the opposite is observed for higher Ti values (~>30 ppm; Fig. 6a). Twenty-nine compositional analyses across fifteen rutile grains give Zr concentrations that range from 242–1087 ppm (Table SM8). These grains yield Zr-in-rutile temperatures of 709–857 °C using a pressure of 28 kbar based on *P-T* estimates of other Oiatabu eclogites (DesOrmeau, 2016). Variations along a transect of a large (~2 mm) matrix rutile (r1) show rim analyses of 718–743 °C and cores yielding 777–788 °C, while other grains give temperatures that vary by upwards of ~70 °C (Fig. 8; Table SM8). Figure 9a suggests a bimodal temperature distribution of ~725 °C and ~780 °C. The lower temperature estimates may result from preserved zoning due to post-peak partial–complete resetting of Zr concentrations; however, expulsion of Zr and subsequent zircon formation was not observed (c.f. Ewing et al., 2013). Trace-element analyses across three separate subhedral–anhedral garnet show minor variation in LREE with flat to negative MREE–HREE profiles (Lu_N/Gd_N = 0.59–6.43, n=20; Table SM9) that reflect minor core to rim zoning in HREE (Fig. 10). Garnet do not record Eu anomalies (Eu/Eu* = 0.83–1.02, n = 20; Table SM9).

Mailolo Dome eclogites

Mailolo Dome eclogite PNG09-041c zircon give consistent depleted HREE values ($Lu_N/Gd_N \leq$ 1), absent Eu anomalies (Eu/Eu* = 0.77–1.40), and Ti concentrations that range from 3–74 ppm corresponding to temperatures of 650–975 ºC (Figs 6b, 8, SM1 and SM2; Tables SM4, SM5, and SM7). Figure 9b shows a dominant peak at ~800 ºC. A single inherited analysis (PNG09-041c_13, ~36 Ma) has a steep HREE pattern ($Lu_N/Gd_N \sim 54$), an absent Eu anomaly, and the lowest Ti concentration (Fig. 6b; Table SM5). Most of the intragrain analyses have similar REE patterns, but large variations in calculated Ti-in-zircon temperatures (~100 ºC) (Figs 6b, 8 and 9b; Tables SM5 and SM7). An increase in overall zircon LREE–MREE abundances correlates with an increasingly negative HREE slope and higher Ti concentrations (Fig. 6b). Th/U ratios span from 0.27–0.80, with the highest ratios associated with the highest Ti concentrations (Fig. SM1; Tables SM5 and SM7). Analyses of thirty-one rutile grains have Zr contents that range from 485–886 ppm (Table SM8) resulting in temperatures of 772–834 ºC (Fig. 8) assuming a pressure of 28 kbar from the nearby coesite eclogite within Mailolo Dome (Baldwin et al., 2008; DesOrmeau et al., 2017). Rutile inclusions and matrix grains yield a single temperature population of ~780 ºC (Figure 9a; Table SM8). *In situ* plagioclase symplectite analyses show minor enrichment in LREE compared to MREE, distinct positive Eu anomalies (Eu/Eu* = 2.52–27.95, n=5), and very low HREE, with most below detection limit (Fig. 10; Table SM9).

Eclogite PNG09-039b zircon show mainly depleted HREE slopes ($Lu_N/Gd_N < 2$), with some steep slopes ($Lu_N/Gd_N = 4–16$; Figs 6c, SM1 and SM2; Tables SM4 and SM5). Most analyses have absent Eu anomalies, with a few grains displaying small negative Eu anomalies (Eu/Eu* = 0.68–2.14; Figs 6c, SM1 and SM2; Tables SM4 and SM5). Like PNG09-041c zircon, the highest Ti results correlate with higher LREE–MREE contents with a negative HREE slope. Titanium concentrations within zircon range from 8–79 ppm corresponding to temperatures of 720–985 °C (Figs 6c and 8; Tables SM5 and SM7) with a generally bimodal temperature distribution of ~760 ºC and ~830 ºC (Fig. 9b). Calculated Ti-in-zircon temperatures within single grains vary from

~10–200 °C (Fig. 8), and Th/U spans from 0.17 to 0.77. The darkest CL sector zones consistently record the highest temperatures (942–985 °C; Fig. 6c) and the highest Th/U ratios (0.72–0.77), which span from 0.17 to 0.77 (Figs 6c and SM1; Tables SM5 and SM7).

Goodenough Dome eclogite and garnet amphibolite

Zircon from garnet amphibolite PNG10-035a and eclogite PNG12-82a yield similar consistent depleted HREE patterns ($Lu_N/Gd_N < 3$), negative to absent Eu anomalies (Eu/Eu* = 0.55–1.05), and Th/U ratios of 0.055–0.59 (Figs 6d, SM1, and SM2; Tables SM4 and SM5). In contrast to zircon from Oiatabu and Mailolo Dome eclogites, Goodenough zircon records Ti concentrations with considerably less scatter, with values ranging from 5–14 ppm and Ti-in-zircon temperatures of 680–780 °C with unimodal temperature populations of ~740 ºC (Fig. 9b). Temperatures vary ~60 °C within a single grain (Figs 6d and 8; Tables SM5 and SM7). Rutile compositions were measured within nineteen grains from PNG10-035a and seventeen grains from PNG12-82a (Table SM8). Rutile Zr contents range from 1360–2920 ppm in PNG10-035a and 1285–1720 ppm in PNG12-82a (Table SM8). Zr-in-rutile temperatures span from 820–910 °C (PNG10-035a) and 815–845 °C (PNG12-82a) (Fig. 8; Table SM8), respectively, assuming a pressure of 16 kbar for both samples calculated for similar mafic samples from northern and southern Goodenough Dome (Davies & Warren, 1992). Single-grain analyses show temperatures that vary up to 90 °C for PNG10-035a, with peak temperatures of ~865 ºC, whereas PNG12-82a reveals little scatter in temperatures (~30 °C), with peak temperatures of ~825 ºC (Fig 9a). Garnet *in situ* trace-element analyses of euhedral grains (n = 3) from garnet amphibolite PNG10-035a have minor LREE variations, consistent MREE, and flat to negative HREE slopes. The HREE patterns reveal minor zoning with more negative slopes towards the rims (Lu_N/Gd_N = 0.48–3.84, n = 23;

Fig. 10; Table SM9). Subhedral garnet (n = 3) from eclogite PNG12-82a shows similar LREE and MREE patterns to PNG10-035a garnet, but slightly positive HREE slopes (Lu_N/Gd_N = 2.06–5.82, n=22; Table SM9). Garnet from both samples yield slightly negative to no Eu anomalies (Eu/Eu* = 0.72–1.02; Fig. 10; Table SM9). Matrix plagioclase *in situ* analyses have an overall enrichment in LREE compared to MREE with positive Eu anomalies (Eu/Eu* = 9.45–54.65, n = 9; Fig. 10; Table SM9).

Oiatabu host gneiss and dikes

Analysis by TIMS-TEA of host-gneiss samples (PNG12-85a, 87a, 92a) reveal zircon REE patterns enriched in HREE (Lu_N/Gd_N = 9–170), Th/U ratios ranging from 0.10 to 0.84 (single analysis << 0.01), and dominantly negative Eu anomalies (Eu/Eu* = 0.19–0.71, except for two absent Eu anomalies of 0.82 and 1.00) (Fig. SM3; Table SM6). There are no trends observed in HREE abundances or Eu/Eu* between inherited grains versus (re)crystallized Pliocene zircon tips.

Trace-element analyses of zircon from weakly deformed dikes yield abnormal REE patterns (e.g. variability in LREE–MREE). These are due to low concentrations attributed to their very small size. Zircon from the weakly deformed dike PNG12-87b shows variable HREE slopes (Lu_N/Gd_N = 3–587), mostly absent Eu anomalies (Eu/Eu* = 0.69–2.33), and low Th/U ratios from 0.01–0.25 (Fig. SM3; Table SM6). The other weakly deformed dike, PNG12-92b, yields zircon REE patterns that have moderate to steep HREE slopes (Lu_N/Gd_N = 5–62), negative to absent Eu anomalies (Eu/Eu* = 0.27–0.92), and variable Th/U ratios from 0.06 to 0.89 (Fig. SM3; Table SM6). For most of the gneiss and crystallized melt samples, LREE concentrations were below detection limits.

DISCUSSION

Eastern PNG is unique in that the world's youngest known UHP eclogites are currently exhuming within an active rift system (Baldwin et al., 2004, 2008; Wallace et al., 2004, 2014; Monteleone et al., 2007; Webb et al., 2008; Little et al., 2011, 2013; Zirakparvar et al., 2011; Gordon et al., 2012; DesOrmeau et al., 2014; Korchinski et al., 2014; DesOrmeau et al., 2017). Given the rapid tectonic history of this Pliocene UHP terrane, high-precision geochronology is a crucial tool to capture metamorphic, melt-crystallization, and deformational events that occur on sub-million year timescales. U-Pb TIMS-TEA results from this study better resolve the timing of eclogite retrogression, revealing new stages of the exhumation path for multiple domes. Below we describe the results and discuss the similarities and differences in the metamorphic and exhumation history across these gneiss domes.

Temporal evolution of the PNG UHP terrane

Peak pressure and temperature history

Of all the domes, Mailolo Dome hosts the only known coesite eclogite (Baldwin et al., 2008). A recent CA-ID-TIMS study analyzed zircon with inclusions of the peak metamorphic assemblage (Omp, Rt, Grt, Ph; DesOrmeau et al., 2017). Thermobarometry, Zr-in-rutile thermometry, and phase-equilibria calculations together with CA-ID-TIMS zircon results suggest that the Mailolo Dome rocks reached UHP conditions of ~27–31 kbar and ~715 ºC from 6.0 to 5.2 Ma. Combining these dates with a likely prograde ca. 7 Ma garnet Lu-Hf isochron date (Zirakparvar et al., 2011) suggests that the crustal rocks recrystallized at (U)HP depths for ~2 Myr.

The incorporation of Zr into rutile has been shown to be temperature dependent when in equilibrium with the appropriate buffer assemblages (quartz and zircon; Zack et al., 2004; Watson et al., 2006; Tomkins et al., 2007). Rutile thermometry has been successful in recording peak temperatures in ultra-high temperature (≥ 900 ºC) and in (U)HP metamorphic assemblages (e.g. Spear et al., 2006; Baldwin et al., 2007; Baldwin et al., 2008; Luvizotto & Zack, 2009; Kooijman et al., 2012; Zheng et al., 2011; Ewing et al., 2013, Stepanov et al., 2016a; DesOrmeau et al., 2017). The ability of the Zr-in-rutile thermometer to record such high temperatures contradicts experimental diffusion studies that suggest diffusive resetting of Zr in rutile occurs five orders of magnitude faster than Ti in zircon at 900 ºC (Cherniak et al., 2007). The Zr concentrations in rutile from Mailolo and Goodenough Domes in this study mostly do not show any obvious correlation with location (matrix versus inclusion), grain size, or association with retrogression textures. Thus, the highest Zr-in-rutile estimates from the eclogites and garnet amphibolite across the domes are interpreted to record peak temperatures. Zr-in-rutile estimates of peak temperatures transition from ~780 ºC in the eastern Oiatabu and central Mailolo domes to ~825–865 ºC in the western Goodenough Dome (Figs 8 and 9). These results are slighter hotter compared to previous rutile thermometry from the coesite locality and from another core zone eclogite within Mailolo Dome (690–750 ºC, Monteleone et al., 2007; Baldwin et al., 2008; DesOrmeau et al., 2017) and similar to results from other Goodenough eclogites (Monteleone et al., 2007). In contrast to the hotter temperatures, the lower estimates of ~725 ºC from Oiatabu eclogite PNG12-95a may be the result of post-crystallization out-diffusion of Zr from nearby zircon (although zircon has yet to be identified in thin section for this sample) or growth of the rutile rim on the larger grain and other matrix grains during cooling.

Retrogression of eclogites across the D'Entrecasteaux Islands

Overprinting of peak mineral assemblages is prevalent in UHP terranes, as retrogression along the exhumation path drives breakdown of phengite (see below) and omphacite and garnet to diopsidic clinopyroxene, amphibole, and plagioclase, producing coarse- to fine-grained symplectite. In some cases, the eclogites transform entirely into amphibolite-facies mineral assemblages. Eclogites from Oiatabu, Mailolo, and Goodenough Domes show evidence for distinct levels of retrogression. Based on the observed relationships of (re)crystallized zircon to breakdown textures, polyphase inclusions within zircon, and mineral assemblages, we posit that zircon from the studied eclogites and garnet amphibolite tracks these distinct degrees of retrogression and thus the exhumation histories of the domes (Figs 3, 7 and 11).

The oldest zircon comes from Oiatabu eclogite PNG12-95a. Initial retrogression of the peak eclogite-facies assemblage (Grt + Omp + Qz + Rt ± Lws) in this sample is marked by growth of coarse, euhedral amphibole at the expense of garnet and possibly lawsonite. This retrogression stage is followed by variable overprinting of omphacite by symplectite of clinopyroxene, plagioclase, and amphibole and formation of kelyphitic rims of amphibole and plagioclase around garnet. Clinozoisite–epidote is found with amphibole and partially broken down garnet suggesting the former presence of lawsonite at peak pressures. The coarse, euhedral amphibole grains are likely related to one, or multiple stages of infiltration of hydrous fluids or internal fluid generation from the possible breakdown of hydrous lawsonite. CA-ID-TIMS analyses give a narrow range in zircon dates from 4.63–4.58 Ma (Fig. 4). The large, pink zircon is mostly prismatic and typically shows sector zoning and weak oscillatory zoning along rims (Figs 4a and 6a). The rapid zircon (re)crystallization (40 ± 30 k.y.) is likely related to a fluid event that also may have driven growth of the coarse amphibole; however, directly linking zircon (re)crystallization to this fluid is challenging because zircon has yet to be identified in thin section to confirm whether it occurs texturally with retrogressed or peak phases. The Ab + Qz polyphase inclusions and amphibole embayments within zircon suggest the zircon formed during retrogression.

To the west, the two eclogites analyzed in Mailolo Dome show similar breakdown of the peak garnet and omphacite assemblage, with amphibole growth along garnet rims and extensive replacement of omphacite by clinopyroxene and plagioclase symplectite. As described above, zircon is mainly found in domains of garnet and omphacite breakdown with retrograde amphibole and plagioclase (Figs 3c and d). Minor zircon is also found as inclusions within garnet in both samples. Zircon from eclogite PNG09-041c gives a CA-ID-TIMS weighted-mean $^{206}Pb/^{238}U$ age of 4.63 ± 0.01 Ma (Fig. 4) that overlaps with the Oiatabu eclogite, whereas zircon from eclogite PNG09-039b yields younger CA-ID-TIMS results of 4.36–4.30 Ma (Fig. 4). Zircon from both samples occurs in domains of extensive retrogression, has similar polyphase inclusion suites (Ksp + Ab+ Qz ± Chl ± Ap ± Cal), and shows mainly sector and oscillatory CL zoning (Fig. 7). The slight difference in timing of initial retrogression (~0.3 Myr) between the eclogite cobble and the *in situ* eclogite may be the result of either structural level (which cannot be definitively assessed) or a difference in timing of metamorphic fluid interaction in different parts of the Mailolo Dome core.

In the far west, Goodenough Dome eclogite and garnet amphibolite are characterized by variable breakdown of garnet to amphibole and plagioclase, low-Na clinopyroxene, and biotite as a matrix phase. Rounded zircon shows weak patchy- and polygonal-sector zones that give the youngest CA-ID-TIMS results across all the domes that overlap from 2.89–2.62 Ma (Fig. 4). Garnet amphibolite PNG10-035a zircon contains a polyphase inclusion of Rt + Bt + Chl + Pl.

This study and previous work on Goodenough eclogites and/or garnet amphibolites document lower pressure mineral assemblages within the mafic rocks in comparison to the other domes (Davies & Warren, 1992; Monteleone et al., 2007). The lower pressure phases preserved in the Goodenough Dome eclogite and garnet amphibolite and the much younger timing of inferred retrogression suggests the western Goodenough Dome may preserve a different *P–T* history compared to the central Mailolo and eastern Oiatabu Domes.

Ti-in-zircon temperatures

Peak Ti-in-zircon temperatures have been reported for the UHT Kaapvaal xenoliths (Baldwin et al., 2007) and Kokchetav UHP diamondiferous rocks (Stepanov et al., 2016a). In comparison, numerous studies of zircon that has crystallized from partial melts report lower Ti-in-zircon temperatures compared to other peak *P–T* estimates suggesting Zr saturation and crystallization occurs upon cooling below peak temperatures (e.g. Baldwin et al., 2007; Kotkova & Harley, 2010; Ewing et al., 2013). Applications of Ti-in-zircon thermometry to UHP terranes is limited by relatively unknown pressure effects of Ti substitution in zircon, as the Ferry & Watson (2007) thermometer is calibrated at ~10 kbar (c.f. Stepanov et al., 2016a).

Oiatabu eclogite PNG12-95a and Mailolo eclogites PNG09-041c and PNG09-039b yield Ti-in-zircon estimates that record considerable variability, with temperature peaks at ~870–1030 ºC, ~800–830 ºC, and ~760 ºC (Fig. 9; Tables SM7). In contrast, Goodenough Dome garnet amphibolite PNG10-035a and eclogite PNG12-82a record lower and more reproducible Ti-in-zircon estimates of ~740 ºC (Fig. 9; Table SM7). Crystal-plastic deformation of zircon can modify the Ti, REE, U, and Th intragrain distribution by the creation of fast-diffusion pathways, potentially causing a decoupling of Ti-in-zircon thermometry and U-Pb geochronology from the conditions and timing of primary crystallization (Timms et al., 2011). Preliminary EBSD data does not show evidence of intragrain deformation. Multiple studies have also documented variable Ti-Si and Ti-Zr substitutions at higher pressures (≥ 10 kbar), which may affect Ti solubility in zircon (Ferriss et al., 2008; Tailby et al., 2011). Thus, the variability and higher Ti-in-zircon temperatures from Mailolo and Oiatabu eclogites likely reflect the unknown pressure effects on Ti substitution. In addition, zircon from Mailolo eclogite PNG09-039b, and in some cases Oiatabu eclogite PNG12-95a, has dark sector CL zones that are correlated with the highest Ti measured concentrations. This could be linked to non-equilibrium effects (e.g. preferential surface adsorption-driven uptake of incompatible elements; Hofmann et al., 2009) in addition to temperature. The limited spatial resolution with LASS hinders proper evaluation of this scenario.

Alternatively, the elevated Ti-in-zircon results (> 800 ºC) recorded by Mailolo and Oiatabu eclogites could represent increased temperatures along the retrogression portion of the *P–T* path and/or fluid infiltration. The increase in temperature may be related to potential interaction with the hot inflowing asthenosphere within the westward propagating Woodlark Rift. Previous *P–T* studies of variably retrogressed PNG eclogites from Mailolo Dome report high temperatures, up to 900 ºC (Fig. 11; Davies & Warren, 1992; Hill & Baldwin, 1993; Baldwin et al., 2004). The variable Ti-in-zircon temperatures from Oiatabu and Mailolo eclogites suggest retrogression temperatures in excess of 800 ºC; however, the cooler Ti-in-zircon temperatures (~740 ºC) from Goodenough Dome may represent zircon crystallization upon cooling from higher peak temperatures (e.g. Kotkova & Harley, 2010; Ewing et al., 2013). It is possible that the lower Ti-in-zircon temperatures for Goodenough Dome may be the result of calculations assuming an overestimate of TiO_2 activity. For example, calculated temperatures increase by ~50 ºC for an assumed $a$$TiO_2$ of 0.6 compared to a value of 1. Despite accounting for variability in $a$$TiO_2$, the temperature discrepancy across the domes remains as all sample estimates would increase with a lower $a\mathrm{TiO_2}$ value. The lower Ti-in-zircon results from Goodenough Dome may represent crystallization of a melt rather than retrogression like Oiatabu and Mailolo Domes considering the proximity to the wet solidus of tonalite (e.g., Schmidt & Thompson, 1996) and the amphibolite-facies mineral assemblages. Due to uncertainty in the unknown pressure effects and the variability related to $a\mathrm{TiO_2}$ and $a\mathrm{SiO_2}$ estimates, the Ti-in-zircon temperatures are taken as a likely relative indicator of increased temperatures (800 ºC) across the terrane during exhumation from UHP conditions.

Partial melting during UHP exhumation

Extensive partial melting associated with UHP exhumation is well-documented for UHP terranes that have experienced high peak–retrograde metamorphic temperatures [Kokchetav, Hermann et al, 2001; Western Gneiss Region, Norway, Labrousse et al., 2002, 2011; Sulu, Wallis et al., 2005; PNG, Little et al., 2011, 2013; Gordon et al., 2012]. The preservation of polyphase inclusions within major peak phases (i.e. garnet, omphacite, kyanite) provide a rare record of fluid-rock interaction at UHP conditions (Hermann & Rubatto, 2014). These inclusions are the primary crystallization products of former silicate and carbonate melts (Stöckhert et al., 2001, 2009; Korsakov & Hermann, 2006; Gao et al., 2012, 2017; Hermann & Rubatto, 2014, Stepanov et al., 2016b). Polyphase inclusions containing diamond found within Kotchetav and Erzgebirge UHP terranes definitively record melting processes occurring under UHP conditions (e.g. Hwang et al., 2001; Stöckhert et al., 2001; Korsakov & Hermann, 2006). Determining *P–T* conditions of formation for polyphase inclusions without UHP mineral indicators (i.e. diamond, coesite) should be done cautiously as (re)crystallization may occur along the exhumation path (e.g.

Stöckhert et al., 2009). For example, Gao et al. (2012) interpret polyphase inclusions of Kfs + Ab + Qtz in garnet from Dabie UHP eclogites to have formed through decompression melting of phengite due to an increase in temperature during exhumation.

Zircon can also armor polyphase inclusions and provide estimates to determine the timing of partial melting. For example, quartzite from the Sulu orogen contains zircon with (U)HP polyphase inclusions consisting of Coe + Qtz + Jd + Pl and ± Qtz ± Pl ± Kfs ± Ms ± Rt; this zircon is interpreted as recording anatectic melting under UHP to lower pressures conditions (Chen et al., 2013). Both Mailolo (U)HP eclogites from this study contain zircon with polyphase inclusions rich in K (Ksp + Ab + Qtz ± Ap ± Chl), whereas zircon from Oiatabu eclogite PNG12-95a has polyphase inclusions of Ab + Qtz and zircon from a Goodenough Dome garnet amphibolite contain a polyphase inclusion of Rt + Pl + Bt +Chl. Of all the samples, minor matrix phengite is only present in Mailolo eclogite PNG09-039b, consistent with local dehydration melting due to increased temperatures during exhumation (Figs 7 and 11; e.g. Zeng et al., 2009; Gao et al., 2012). The variation in the mineral assemblage (Ab + Qtz ± Ksp) of the inclusions may be the result of which hydrous phase broke down (i.e. phengite, paragonite) and/or the influence of externally-derived fluids. While more *P–T* work needs to be completed on these rocks, the abundant polyphase inclusions found within zircon and the elevated temperatures (> 800 ºC) provides strong evidence for partial melting of the (U)HP eclogites in PNG. Combining the zircon textures and inclusion relationships described above suggest the main process responsible for metamorphic zircon growth in all mafic samples was crystallization from a melt or precipitation from a fluid (e.g. Rubatto, 2017).

Zircon trace-element data

Numerous studies have used zircon REE composition, with flat HREE slopes ($Lu_N/Gd_N < 3$) and absent Eu anomalies (Eu/Eu*>0.75), to suggest that zircon (re)crystallized at eclogite-facies conditions (e.g. Rubatto, 2002; Rubatto & Hermann, 2003; Bingen et al., 2004; Baldwin et al., 2004; Mattinson et al., 2006; Monteleone et al., 2007; Rubatto & Hermann, 2007a, 2007b; Gilotti et al., 2013; DesOrmeau et al., 2015). In comparison, zircon that grew during retrogression or in the presence of melt will likely vary from the typical eclogite REE profile, as plagioclase becomes stable (resulting in a negative Eu anomaly) and garnet typically breaks down (resulting in a steep HREE slope).

In this study, solution ICP-MS and *in situ* analyses of zircon from all PNG eclogites yields similar REE patterns with mainly depleted HREEs and absent Eu anomalies (Figs 6, SM1 and SM2). These results suggest zircon (re)crystallization at peak eclogite-facies conditions, consistent with zircon REE patterns reported for other Mailolo and Goodenough Dome eclogites (Baldwin et al., 2004; Monteleone et al., 2007). However, there are multiple lines of evidence that suggest the zircon REE patterns may not record peak conditions. There are no obvious differences in the zircon REE patterns from samples collected across the domes despite the varying degrees of garnet breakdown and plagioclase stability found in the mafic samples. Textures preserved in Mailolo Dome eclogites directly link zircon (re)crystallization to domains of garnet breakdown and symplectite formation, despite that the zircon could be interpreted as recording peak conditions as it has the classic ‘eclogite-facies’ REE patterns. Moreover, strongly deformed leucosomes and sills from similar structural levels within Goodenough Dome reveal zircon (re)crystallization ages with garnet absent and plagioclase stable REE patterns that are older and/or coeval with the zircon ages obtained from the Goodenough eclogite and garnet amphibolite (ca. 3.9–2.8 Ma vs. 2.9–2.6 Ma, respectively; DesOrmeau et al., 2014). The similar ages of melt crystallization, the lower pressure, plagioclase-stable assemblages, and the lower Ti-in zircon temperatures near the wet solidus of tonalite (Schmidt & Thompson, 1996) argue that the zircon documents melt crystallization at (upper) amphibolite-facies conditions within Goodenough Dome mafic samples.

There are multiple possibilities for the flat HREE slopes and absent Eu anomalies revealed from the variably retrogressed eclogite and garnet amphibolite zircon, including: 1) zircon (re)crystallization in all samples took place at eclogite-facies conditions; 2) varying modal amounts and composition of the REE-controlling phases (i.e. garnet and plagioclase; Rubatto, 2017); 3) zircon REE signatures were strongly influenced by original whole rock compositions [depletion in HREE, enrichment in Eu, e.g. HP zircon Kotchetav gneisses, Hermann et al., 2001; Dora Maira whiteschists, Gauthiez-Putallaz et al., 2016]; and/or 4) zircon (re)crystallization in the presence of garnet and melt during exhumation.

It is possible that all the zircon (re)crystallized at peak (U)HP eclogite-facies conditions; however, most zircon in this study is restricted to domains of partially broken down peak phases and matrix symplectite. In addition, the same zircon from Mailolo and Oiatabu eclogites contain polyphase inclusions that include plagioclase. These textural settings suggest that either peak eclogite-facies zircon has been thoroughly erased/recrystallized or zircon growth did not take place until Zr was introduced via breakdown of peak phases or from fluids or melt during retrogression but while still at eclogite-facies conditions (Kohn et al., 2015).

The level of breakdown, modal abundance, and the potential zoning of HREE within garnet may all play a role in controlling REE distribution in zircon (Rubatto, 2017). Garnet breakdown during retrogression across the PNG domes is variable, but samples of Goodenough and Oiatabu eclogites from this study show extensive garnet replacement (resorbed rims and minor core replacement). It is difficult to estimate the degree to which garnet must break down to influence HREE abundance in zircon, but in these rocks, the zircon should incorporate any available HREE, as there is no indication of other competing minerals (e.g. xenotime). If garnet and zircon contain similar concentrations of Eu and HREE, then this suggests the zircon was influenced by the prograde to peak garnet composition rather than by growth during exhumation and likely garnet breakdown conditions. Goodenough samples (PNG12-82a and PNG10-035a) yield garnet and zircon REE patterns with slightly negative to absent Eu anomalies and similar HREE abundances, whereas Oiatabu eclogite PNG12-95a zircon and garnet REE patterns show absent Eu anomalies and zircon HREE enrichment compared to garnet (Fig. 10; Table SM9).

Plagioclase composition and textural occurrence could also have influenced the (re)crystallized zircon REE signatures. Potential differences in REE may exist for plagioclase found within symplectite compared to plagioclase found as a matrix phase. Plagioclase involved in a symplectite reaction may have inherited the REE signature of the phase being replaced (i.e. omphacite) due to limited element mobility. In comparison, matrix plagioclase is typically marked by a positive Eu anomaly. REE analyses of plagioclase within symplectite in Mailolo eclogite PNG09-041c and matrix grains in Goodenough eclogite PNG12-82a show similar REE signatures with distinct positive Eu anomalies, although matrix plagioclase shows more Eu enrichment (Fig. 10; Table SM9). This suggests that zircon (re)crystallization coincident with retrograde plagioclase growth (matrix or symplectite) should be depleted in Eu. The lack of a negative Eu anomaly in zircon from this study suggests plagioclase and zircon growth was not coincident. Alternatively, it is possible that the absent Eu anomalies result from the availability of Eu in the fluid from which zircon (re)crystallizes (e.g. Burnham & Berry, 2012) or it is related to the affinity of zircon for Eu^{3+} in comparison to feldspars that mainly take up Eu^{2+} (e.g. Kohn et al., 2015).

Zircon (re)crystallization related to retrogression could exhibit REE compositions marked by a depletion in HREE and absent Eu anomaly if the bulk rock composition displays such trends (e.g. Hermann et al., 2001; Gauthiez-Putallaz et al., 2016; Rubatto, 2017). Whole-rock REE analyses of three eclogites and a garnet amphibolite from across the domes show absent Eu anomalies and HREE concentrations that overlap with zircon and garnet REE patterns (Fig. 10; Table SM10). Mailolo Dome eclogite PNG09-041c shows an enrichment in LREE and a depletion in HREE, whereas Oiatabu Dome eclogite PNG12-95a records the opposite with a depletion in LREE and a slight enrichment in HREE (Fig. 10). Goodenough Dome samples plot in between these eclogite end-members. There does not appear to be a correlation between degree of retrogression and the variation in the mobile LREE; thus, the bulk-composition differences cannot be explained by amphibolite-facies overprinting. Instead, these differences most likely reflect protolith heterogeneity (i.e. island arc basalts vs. mid-ocean ridge basalts) and/or fluid-melt interactions during the subduction–exhumation history (e.g. Hermann et al., 2006; Spandler et al., 2007; Zhao et al., 2007).

Finally, zircon formed in the presence of garnet and melt can explain the relationship between the polyphase inclusions, whole rock and trace-element patterns from garnet, zircon, and plagioclase, and the observed retrogression textures. The plagioclase in the polyphase inclusions hosted within the zircon crystallized from a melt; therefore, the plagioclase was not a stable phase when the zircon crystallized and must have formed later at amphibolite-facies conditions when the melt crystallized. In this case, the zircon records the timing of melting under garnet-stable, plagioclase-unstable conditions rather than melt crystallization, which is supported by the whole rock and trace element patterns from all phases. The zircon must predate amphibole and plagioclase symplectite formation that is likely related to aqueous fluid release during hydrous melt crystallization. Further study is necessary to determine when the coarser amphibole grew relative to the symplectite.

In summary, the zircon REE patterns from the PNG samples are interpreted to represent (re)crystallization at eclogite-facies conditions during exhumation and partial melting from 4.6–4.3 Ma within Mailolo and Oiatabu Domes. This occurred prior to extensive retrogression of peak (U)HP phases and the crystallization of lower pressure plagioclase. Zircon growth within Goodenough Dome mafic rocks is interpreted to represent melt crystallization at 2.9–2.6 Ma under lower pressure amphibolite-facies conditions.

Exhumation within an active rift

Based on a suite of petrologic, structural, geophysical, and geochronology data, Little et al. (2011) proposed that the onset of Pliocene seafloor spreading and westward-propagating rifting within the Woodlark basin caused subducted continental crust to (re)crystallize under UHP conditions and detach from the remnant slab. Inherited zircon dates of ca. 90–53 Ma from two orthogneisses in the Oiatabu Dome carapace (PNG12-87a, PNG12-92a) further support the suggestion that Cretaceous–Paleogene Australian plate material is the protolith for the lower plate gneisses and eclogites (Davies, 1980; Davies & Jacques, 1984; Davies & Warren, 1988; Hill & Baldwin, 1993; Baldwin & Ireland, 1995; Gordon et al., 2012; Zirakparvar et al., 2013; DesOrmeau et al., 2014). Pressure-temperature-time results indicate the eclogite-bearing crust was exhumed from mantle depths at plate-tectonic rates (≥2.3 cm/yr; Davies & Warren, 1988; Hill & Baldwin, 1993; Baldwin et al., 2004; DesOrmeau et al., 2017). During initial exhumation, the rocks may have experienced increased temperatures (Ti-in-zircon estimates > 800 ºC) facilitating local dehydration melting in both the gneiss and the eclogite. Continued exhumation to the base of the crust was thus aided by this buoyant partial melting (Ellis et al., 2011; Little et al., 2011). The UHP terrane may have slowed in its ascent due to the achievement of neutral buoyancy with the surrounding material at the base of the crust. Further exhumation within the lower-to-middle crust was likely facilitated by ductile thinning (Ellis et al., 2011; Little et al., 2011). Final emplacement of the domes within the upper crust was assisted by melt-induced buoyancy (Hill et al, 1995; Ellis et al., 2011; Gordon et al., 2012; DesOrmeau et al., 2014) and ultimately was accomplished by tectonic extension in the upper crust (Tregoning et al., 1998; Taylor et al, 1999; Abers 2001; Abers et al., 2002; Taylor & Huchon, 2002; Wallace et al., 2004, 2014; Kington & Goodliffe, 2008; Eilon et al., 2014, 2015). Below, the different phases of exhumation and the individual deformation history for the three domes, from east to west, are discussed.

Eastern Oiatabu Dome

The ca. 4.6 Ma dates from the carapace eclogite in Oiatabu Dome mark the timing of initial retrogression from peak *P–T* conditions of ~780 ºC/~28 kbar and the first record of eclogite partial melting and retrogression across the domes (Fig. 11). Increased temperatures during exhumation indicated by Ti-in-zircon results > 800 ºC likely resulted in breakdown of hydrous lawsonite and partial melting and formation of hydrous melt polyphase inclusions in zircon. Coarse amphibole grew at some time during or after this event. Host gneiss PNG12-85a within Oiatabu Dome reveals coeval metamorphism from ca. 5.7–4.5 Ma at lower pressures (zircon enriched in HREE, variable Eu anomalies) structurally higher within the dome (Fig. 5).

Two crosscutting, weakly deformed felsic dikes from similar structural levels of the carapace represent waning ductile deformation and melt crystallization from ca. 3.0–2.9 Ma (Fig. 5). Trace-element compositions of zircon from the dikes record variable HREE enrichment and a wide range in Eu anomalies and Th/U ratios. This large variation may be attributed to partial resetting of protolith zircon and/or analytical uncertainty associated with low REE concentrations. Given that they are weakly deformed, these dikes record one of the latest melt-crystallization events prior to upper crustal exhumation.

In comparison, ~20 km to the south in Normanby Dome, maximum ages for retrogression within carapace host gneisses are similar (ca. 5.6–5.0 Ma) to the Oiatabu Dome gneiss. Strongly deformed granodiorite sills record melt crystallization at ca. 4.1 Ma, and ductile deformation ended at ca. 2.9 Ma (DesOrmeau et al., 2014). No mafic eclogite has been dated from Normanby Dome.

Central Mailolo Dome

Prograde–peak UHP metamorphism within Mailolo Dome occurred from ca. 7.0–5.2 Ma (Zirakparvar et al., 2011; DesOrmeau et al., 2017). The timing of initial retrogression from peak *P–T* conditions of ~28 kbar (Baldwin et al., 2004; DesOrmeau et al., 2017) and ~780 ºC and partial melting of eclogites PNG09-041c and PNG09-039b occurred at ca. 4.6–4.3 Ma. Similar to Oiatabu Dome, Mailolo may have experienced increased temperatures during initial exhumation (> 800 ºC; Ti-in-zircon) causing breakdown of phengite and dehydration melting (Fig. 11). Strongly deformed leucosomes that share the same amphibolite-facies fabric as the host gneiss record melt crystallization near the base of the crust in the plagioclase stability field ~1.0 Myr later, from ca. 3.5–3.0 Ma (Gordon et al., 2012) suggesting exhumation of (U)HP rocks within

Mailolo Dome from ~28 kbar to <16 kbar in ~2 Myr. Dikes within Mailolo Dome record an end to ductile deformation at ca. 2.4 Ma (Gordon et al., 2012).

Western Goodenough Dome

The westernmost exposed eclogite and garnet amphibolite from Goodenough Dome show evidence for extensive retrogression and crystallization from a melt, respectively. Therefore, the peak metamorphic conditions for the Goodenough Dome are difficult to determine (Fig. 11). The oldest dates are from strongly deformed leucosomes that crystallized at ca. 3.9–2.8 Ma, presumably as the (U)HP rocks reached the lower crust (DesOrmeau et al., 2014). Retrogression and partial melting of the eclogite and garnet amphibolite from inferred peak *P–T* conditions of ~16 kbar (minimum estimate; Davies and Warren, 1992) and ~825–865 ºC (Zr-in-Rutile) likely occurred in the lower crust, as indicated by the youngest zircon (re)crystallization of all the studied eclogites in PNG at ca. 2.8–2.6 Ma and host gneiss metamorphic ages of ca. 2.7–2.6 Ma (SIMS zircon weighted-mean $^{206}Pb/^{238}U$ dates; Baldwin & Ireland, 1995). Results from leucosomes, host gneisses, inclusions within zircon (Rt + Pl + Bt + Chl), and from breakdown textures observed in the eclogite and garnet amphibolite suggest samples from this and previous studies (ca. 2.9–2.6 Ma eclogites; Monteleone et al., 2007) likely record a combination of retrogression and melt crystallization under amphibolite-facies conditions and not peak eclogite-facies conditions.

The degree of retrogression and/or melt crystallization (i.e. garnet breakdown, abundant plagioclase) and the ~2.0–1.5 Myr younger zircon ages of the Goodenough Dome eclogites and garnet amphibolite compared to those studied to the east suggest the Goodenough mafic samples: 1) may have resided in the lower–to–middle crust longer and underwent more extensive partial melting and retrogression of peak phases; 2) did not reach the same peak *P–T* conditions as the other higher-pressure eclogites that contain coesite, kyanite, and /or phengite; or 3) low Na and Si bulk-rock compositions may have resulted in a lack of omphacite and other peak phases (i.e. Davies & Warren, 1992). Previous pressure estimates (~20–25 kbar) for Goodenough eclogites indicate that the rocks did not experience high pressures like Mailolo Dome (Davies & Warren, 1992); however, Zr-in-rutile and previous thermometry estimates suggest the rocks reached temperatures > 850 ºC (Davies & Warren, 1992; Monteleone et al., 2007; this study). The Ti-in-zircon results show that the rocks of Mailolo and Oiatabu Domes also experienced these elevated temperatures, but likely during post-peak metamorphism and perhaps for a much shorter time in comparison to Goodenough Dome rocks. The lack of omphacite, extensive amphibolite-facies assemblages, and evidence for only high peak temperatures (Zr-in-rutile) support that the Goodenough Dome rocks may have interacted or been affected by rifting more extensively than the other domes.

The exhumation of the Goodenough HP rocks continued with the crystallization of the pegmatite that intruded garnet amphibolite PNG10-035a at ca. 2.6–2.4 Ma. Similar to Mailolo Dome, ductile deformation ended by ca. 2.3 Ma. Emplacement of all domes across the D'Entrecasteaux Islands within the brittle upper crust is recorded by non-deformed pluton and dike crystallization by 1.8 Ma (Baldwin et al., 1993; DesOrmeau et al., 2014).

CONCLUSION

High-precision U-Pb zircon dates track the exhumation history of eclogites, garnet amphibolite, and the host migmatitic rocks exposed within gneiss domes across the eastern PNG UHP terrane. Polyphase inclusions within zircon, trace-element thermometry, and trace-element signatures provide the first documented evidence for partial melting of the eclogites within Mailolo and Oitabu Domes during exhumation. The combination of inclusion and textural evidence, and for Goodenough, the age of leucosomes, argue that the zircon records the timing of partial melting and retrogression rather than peak metamorphism across the domes. Initial exhumation, the breakdown of peak mineral assemblages, and associated partial melting occurred at ca. 4.6 Ma in Oiatabu Dome and down to ca. 4.3 Ma in Mailolo Dome. The host gneiss within Oiatabu Dome underwent metamorphism from ca. 5.7–4.5 Ma at higher structural levels compared to eclogite retrogression. Late melt crystallization associated with syn-exhumational ductile deformation within Oiatabu Dome occurred at ca. 3.0–2.9 Ma. To the west, Goodenough Dome eclogite and garnet amphibolite preserve lower-pressure mineral assemblages and record melt crystallization and retrogression at ca. 2.9–2.6 Ma, which is likely the result of more prolonged interaction with rift-related fluids and/or residence within the lower crust. All domes record final non-deformed melt crystallization at ca. 1.8 Ma. This study highlights the advantages of combining solution and *in situ* zircon REE data with trace-element thermometry (Zr-in-rutile, Ti-in-zircon), major mineral and whole-rock REE data, and detailed petrological evidence to better interpret high-precision and high-spatial resolution zircon U-Pb dates from variably retrogressed (U)HP eclogites. These results document the complicated retrogression and partial melting history across three of the domes following peak UHP metamorphism and the rapid nature of exhumation for the Pliocene PNG UHP terrane that ascended from the upper mantle to Earth's surface in ~2–3 Myr.

ACKNOWLEDGEMENTS

We would like to thank Jahan Ramezani for assistance in the MIT Isotope Laboratory over multiple visits and Johannes Hammerli for assistance in collecting the trace element analyses of plagioclase at the University of Western Australia. The manuscript benefited from insightful and constructive comments from C. Mattinson, A. Zirakparvar, and an anonymous reviewer. J. Hermann provided excellent editorial handling and suggestions for improvement of the manuscript. Lawrence Livermore National Laboratory is operated by Lawrence Livermore National Security, LLC, for the U.S. Department of Energy, National Nuclear Security Administration under Contract DE-AC52-07NA27344.

FUNDING

This work was supported by National Science Foundation [EAR-1062187 to S.M.G.] and a Marsden Fund Grant [08-VUW-020 to T.A.L.]. High-precision mass spectrometry at MIT is possible because of a National Science Foundation Instrumentation and Facilities Grant [EAR-0931839 to S.A.B] and the collective sharing of knowledge by the EARTHTIME community.

REFERENCES

Abers, G.A. (2001). *Evidence for seismogenic normal faults at shallow depths in continental rifts*. In: Wilson, R.C.L., R.B. Whitmarsh, B. Taylor, N. Froitzham, (Eds.) *Non-volcanic Rifting of Continental Margins*, The Geological Society of London, Special Publications **187**, 305–318, London.

Abers, G.A., Ferris, A., Craig, M., Davies, H., Lerner-Lam, A.L., Mutter, J.C. & Taylor, B. (2002). Mantle compensation of active metamorphic core complexes at Woodlark rift in Papua New Guinea. *Nature* **418**, 862–865, doi:10.1038/nature00990.

Amato, J.M., Johnson, C., Baumgartner, L. & Beard, B. (1999). Sm–Nd geochronology indicates rapid exhumation of Alpine eclogites. *Earth and Planetary Science Letters* **171**, 425–438.

Baldwin, S.L. & Ireland, T.R. (1995). A tale of two eras: Pliocene-Pleistocene unroofing of Cenozoic and late Archean zircons from active metamorphic core complexes, Solomon Sea, Papua New Guinea. *Geology* **23**, 1023–1026, doi: 10.1130/0091-7613(1995)023<1023:ATOTEP>2.3.CO;2.

Baldwin, S.L. & Das, J.P. (2015). Atmospheric Ar and Ne returned from mantle depths to the Earth's surface by forearc recycling. *Proceedings of the National Academy of Sciences* **112(46)**, 14174–14179, doi:10.1073/pnas.1424122112.

Baldwin, J.A., Brown, M., & Schmitz, M.D. (2007). First application of titanium-in-zircon thermometry to ultrahigh-temperature metamorphism. *Geology* ***35*****(4)**, 295-298.

Baldwin, S.L., Lister, G.S., Hill, E.J., Foster, D.A. & McDougall I. (1993). Thermochronologic constraints on the tectonic evolution of active metamorphic core complexes, D'Entrecasteaux Islands, Papua New Guinea. *Tectonics* **12**, 611–628, doi: 10.1029/93TC00235.

Baldwin, S.L., Monteleone, B., Webb, L.E., Fitzgerald, P.G., Grove, M. & Hill, E.J. (2004). Pliocene eclogite exhumation at plate tectonic rates in eastern Papua New Guinea. *Nature* **431**, 263–267, doi:10.1038/nature02846.

Baldwin, S.L., Webb, L.E. & Monteleone, B.D. (2008). Late Miocene coesite-eclogite exhumed in the Woodlark Rift. *Geology* **36**, 735–738, doi: 10.1130/G25144A.1.

Bingen, B., Austrheim, H., Whitehouse, M.J. & Davis, W.J. (2004). Trace element signature and U–Pb geochronology of eclogite-facies zircon, Bergen Arcs, Caledonides of W Norway. *Contributions to Mineralogy and Petrology* **147**, 671–683, http://dx.doi.org/10.1007/s00410-004-0585-z.

Bohlen, S.R. & Boettcher, A.L. (1982). The quartz⇆ coesite transformation: a precise determination and the effects of other components. *Journal of Geophysical Research: Solid Earth* **87(B8)**, 7073–7078.

Bousquet, R., Oberhänsli, R., Goffé, B., Wiederkehr, M., Koller, F., Schmid, S.M. & Martinotti, G. (2008). Metamorphism of metasediments at the scale of an orogen: a key to the Tertiary geodynamic evolution of the Alps*. *Geological Society, London, Special Publications* **298(1)**, 393–411.

Bowring, J.F., McLean, N.M. & Bowring, S.A. (2011). Engineering cyber infrastructure for U–Pb geochronology: Tripoli and U–Pb redux. *Geochemistry, Geophysics, Geosyst*ems **12**, Q0AA19, http://dx.doi.org/10.1029/2010GC003479.

Burnham, A.D. & Berry, A.J. (2012). An experimental study of trace element partitioning between zircon and melt as a function of oxygen fugacity. *Geochimica et Cosmochimica Acta* **95**, 196–212.

Cairns, E.A., Little, T.A., Turner, G.M., Wallace, L.M. & Ellis, S. (2015). Paleomagnetic evidence for vertical-axis rotations of crustal blocks in the Woodlark Rift, SE Papua New Guinea: Miocene to present-day kinematics in one of the world's most rapidly extending plate boundary zones. *Geochemistry, Geophysics, Geosystems* **16(7)**, 2058-2081.

Chen, Y.X., Zheng, Y.F. & Hu, Z. (2013). Petrological and zircon evidence for anatexis of UHP quartzite during continental collision in the Sulu orogen. *Journal of Metamorphic Geology* **31(4)**, 389-413.

Cherniak, D.J., Manchester, J., Watson, E.B. (2007). Zr and Hf diffusion in rutile. *Earth Planetary and Science Letters* **261(1–2)**, 267-279.

Chopin, C. (1984). Coesite and pure pyrope in high-grade blueschists of the western Alps: a first record and some consequence. *Contributions to Mineralogy and Petrology* **86**, 107-118, doi: 10.1007/BF00381838.

Cloos, M., Sapiie, B., vanUfford, Q.A., Weiland, R.J., Warren, P.Q. & McMahon, T.P. (2005). Collisional delamination in New Guinea: the geotectonics of slab break-off. *Geological Society of America Special Paper 400* **51**, doi: 10.1130/2005.2400.

Condon, D.J., Schoene, B., McLean, N.M., Bowring, S.A. & Parrish, R.R. (2015). Metrology and traceability of U–Pb isotope dilution geochronology (EARTHTIME Tracer Calibration Part I). *Geochimica et Cosmochimica Acta* **164**, 464–480, doi:10.1016/j.gca.2015.05.026.

Corfu, F., Hanchar, J.M., Hoskin, P.W.O. & Kinny, P. (2003). *Atlas of zircon textures*. In: Hanchar, J.M. and Hoskin P.W.O. (eds.), *Zircon Reviews in Mineralogy and Geochemistry* **53**, 468–500. Washington, DC: Mineralogical Society of America.

Davies, H.L. (1973). The Geology of Fergusson Island, map with explanatory notes. Australia Bureau of Mineral Resources.

Davies, H.L. (1980). Crustal structure and emplacement of ophiolite in southeastern Papua New Guinea. *Colloques Internationaux du C.N.R.S* **272**, 17–33.

Davies, H.L. (1990). *Structure and evolution of the border region of New Guinea*. In: Carman, G.J., Z. Carman, (Eds.), Petroleum Exploration in Papua New Guinea: *Proceedings of the First PNG Petroleum Convention, Port Morseby, February 12–14, 1990*, 249–269.

Davies H.L. (2012). The geology of New Guinea: the cordilleran margin of the Australian continent. *Episodes* **35**, 87–102.

Davies, H.L. & Jaques, A.L. (1984). Emplacement of ophiolite in Papua New Guinea. *Geological Society of London Special Publication 13*, 341–350, doi: 10.1144/GSL.SP.1984.013.01.27.

Davies, H.L. & Warren, R.G. (1988). Origin of eclogite-bearing, domed, layered metamorphic complexes (core complexes) in the D'Entrecasteaux Islands, Papua New Guinea. *Tectonics* **7**, 1–21, doi: 10.1029/TC007i001p00001.

Davies, H.L. & Warren, R.G. (1992). Eclogites of the D'Entrecasteaux Islands, *Contributions to Mineralogy and Petrology* **112**, 463–474, doi: 10.1007/BF00310778.

Davies, H.L. & Williamson, A.N. (1998). Buna, Papua New Guinea, 1:250,000 Geological Series, *Geological Survey of Papua New Guinea Explanatory Notes SC/55-3.*, Port Moresby, Papua New Guinea.

de Sigoyer, J., Chavagnac, V., Blichert-Toft, J., Villa, I. M., Luais, B., Guillot, S., Cosca, M. & Mascle, G. (2000). Dating the Indian continental subduction and collisional thickening in the northwest Himalaya: Multichronology of the Tso Morari eclogites. *Geology* **28(6)**, 487–490.

DesOrmeau, J.W., Gordon, S.M. Little, T.A. & Bowring, S.A. (2014). Tracking the exhumation of a Pliocene (U)HP terrane: U-Pb and trace-element constraints from zircon, D'Entrecasteaux Islands, Papua New Guinea, *Geochemistry, Geophysics, Geosystems* **15**, doi:10.1002/2014GC005396.

DesOrmeau, J.W., Gordon, S.M., Kylander-Clark, A.R., Hacker, B.R., Bowring, S.A., Schoene, B. & Samperton, K.M. (2015). Insights into (U) HP metamorphism of the Western Gneiss Region, Norway: A high-spatial resolution and high-precision zircon study. *Chemical Geology* **414**, 138–155, http://dx.doi.org/10.1016/j.chemgeo.2015.08.004.

DesOrmeau, J.W. (2016). *Temporal and Petrological Constraints of Ultrahigh-Pressure Metamorphism and Exhumation of Crustal Material from Mantle Depths to Earth's Surface: Insights from a Large and Small UHP Terrane*, Department of Geological Sciences and Engineering **10125999**, University of Nevada, Reno, Nevada.

DesOrmeau, J.W., Gordon, S.M., Little, T.A., Bowring, S.A. & Chatterjee, N. (2017). Rapid time scale of Earth's youngest known ultrahigh-pressure metamorphic event, Papua New Guinea. *Geology* **45(9)**, 795-798, doi:10.1130/G39296.1

Eilon, Z., Abers, G.A., Jin, G. & Gaherty, J.B. (2014). Anisotropy beneath a highly extended continental rift. *Geochemistry, Geophysics, Geosystems* **15**, 545–564, doi:10.1002/2013GC005092.

Eilon, Z., Abers, G.A., Gaherty, J.B. & Jin, G. (2015). Imaging continental breakup using teleseismic body waves: The Woodlark Rift, Papua New Guinea. *Geochemistry, Geophysics, Geosystems* **16**, doi:10.1002/2015GC005835.

Ellis, S.M., Little, T.A., Wallace, L.M., Hacker, B.R. & Buiter, S.J.H. (2011). Feedback between rifting and diapirism can exhume ultrahigh-pressure rocks. *Earth and Planetary Science Letters* **311**, 427–438, doi: 10.1016/j.epsl.2011.09.031.

Ernst, W. G., Maruyama, S., & Wallis, S. (1997). Buoyancy-driven, rapid exhumation of ultrahigh-pressure metamorphosed continental crust: *Proceedings of the National Academy of Sciences*, U.S.A., **94**, 9532–9537.

Ernst, W.G. (2001). *Subduction, ultrahigh-pressure metamorphism, and regurgitation of buoyant crustal slices – implications for arcs and continental growth*. In: Rubie, D. & van der Hilst, R. (Eds.), *Processes and Consequences of Deep Subduction* 253–275, doi : 10.1016/S0031-9201(01)00231-X.

Ewing, T., Hermann, J., & Rubatto, D. (2013). The robustness of the Zr-in-rutile and Ti-in-zircon thermometers during high-temperature metamorphism (Ivrea-Verbano Zone, northern Italy). *Contributions to Mineralogy and Petrology* **165**, 757–779.

Faccenda, M., Minelli, G. & Gerya, T.V. (2009). Coupled and decoupled regimes of continental collision: Numerical modeling. *Earth and Planetary Science Letters* **278**, 337–349, doi:10.1016/j.epsl.2008.12.021.

Ferriss, E.D.A., Essene, E.J., Becker, U. (2008). Computational study of the effect of pressure on the Ti-in-zircon geothermometer. *European Journal of Mineralogy* **20**,745–755.

Ferry, J.M. & Watson, E.B. (2007). New thermodynamic models and revised calibrations for the Ti-in-zircon and Zr-in-rutile thermometers *Contributions to Mineralogy and Petrology* **154**, 429–437.

Fitzgerald, P.G., Baldwin, S.L., Miller, S.L., Perry, S.E., Webb, L.E. & Little, T.A. (2008), Low temperature constraints on the evolution of metamorphic core complexes of the Woodlark rift system. *Annual Meeting of the American Geophysical Union. AGU, EOS Transactions*, San Francisco, CA.

Gao, X.Y., Zheng, Y.F., & Chen, Y.X. (2012). Dehydration melting of ultrahigh-pressure eclogite in the Dabie orogen: evidence from multiphase solid inclusions in garnet. *Journal of Metamorphic Geology* **30(2)**, 193-212.

Gao, X.Y., Chen, Y.X., & Zhang, Q.Q. (2017). Multiphase solid inclusions in ultrahigh-pressure metamorphic rocks: A snapshot of anatectic melts during continental collision. *Journal of Asian Earth Sciences* **145**, 192-204.

Gauthiez-Putallaz, L., Rubatto, D., & Hermann, J. (2016). Dating prograde fluid pulses during subduction by in situ U–Pb and oxygen isotope analysis. *Contributions to Mineralogy and Petrology* **171**, 15.

Gebauer, D., Schertl, H.P., Brix, M. & Schreyer, W. (1997). 35 Ma old ultrahigh-pressure metamorphism and evidence for very rapid exhumation in the Dora Maira massif, Western Alps. *Lithos* **41**, 5–24, doi: 10.1016/S0024-4937(97)82002-6.

Gerya, T.V., Perchuk, L.L. & Burg, J.P. (2008). Transient hot channels: perpetrating and regurgitating ultrahigh-pressure, high temperature crust-mantle associations in collision belts. *Lithos* **103**, 236–256.

Gilotti, J.A. (2013). The realm of ultrahigh-pressure metamorphism. *Elements* **9**, 255–260.

Gordon, S.M., Little, T.A., Hacker, B.R., Bowring, S.A., Baldwin, S.L. & Kylander-Clark, A.R.C (2012). Multi-stage exhumation of young UHP–HP rocks: timescales of melt crystallization in the D'Entrecasteaux Islands, southeastern Papua New Guinea, *Earth and Planetary Science Letters* **351–352**, 237–246, doi: 10.1016/j.epsl.2012.07.014.

Hacker, B.R., Calvert, A.T., Zhang, R.Y., Ernst, W.G. & Liou, J.G. (2003). Ultrarapid exhumation of ultrahigh pressure diamond-bearing metasedimentary and meta-igneous rocks of the Kokchetav Massif. *Lithos* **70**, 61–75.

Hacker, B.R., Wallis, S.R., Ratschbacher, L., Grove, M., & Gehrels, G. (2006). High-temperature geochronology constraints on the tectonic history and architecture of the ultrahighpressure Dabie–Sulu orogen. *Tectonics* **25**, TC5006. doi:10.1029/2005TC001937.

Hacker, B.R. (2007). *Ascent of the ultrahigh-pressure Western Gneiss Region, Norway*. In: Cloos, M., Carlson, W.D., Gilbert, M.C., Liou, J.G. & Sorenson, S.S. (Eds.), Convergent Margin Terranes and Associated Regions, A Tribute to W.G. Ernst, *Geological Society of*

America Special Paper **419,** Geological Society of America, Boulder, CO, 171–184, doi: 10.1130/2006.2419(09).

Hermann, J., & Rubatto, D. (2014). Subduction of continental crust to mantle depth: geochemistry of ultrahigh-pressure rocks. In *Treatise on Geochemistry, 2nd Edition*. Elsevier.

Hermann, J., Rubatto, D., Korsakov, A. & Shatsky, V.S. (2001). Multiple zircon growth during fast exhumation of diamondiferous, deeply subducted continental crust (Kokchetav Massif, Kazakhstan). *Contributions to Mineralogy and Petrology* **141**, 66–82, doi: 10.1007/s004100000218.

Hermann, J., Spandler, C., Hack, A., & Korsakov, A.V. (2006). Aqueous fluids and hydrous melts in high-pressure and ultra-high pressure rocks: implications for element transfer in subduction zones. *Lithos* **92(3-4)**, 399-417.

Hill, E.J. (1994). Geometry and kinematics of shear zones formed during continental extension in eastern Papua New Guinea. *Journal of Structural Geology* **16**, 1093–1105, doi: 10.1016/0191-8141(94)90054-X.

Hill, E.J. & Baldwin, S.L. (1993). Exhumation of high-pressure metamorphic rocks during crustal extension in the D'Entrecasteaux region: Papua New Guinea. *Journal of Metamorphic Geology* **11**, 261–277, doi: 10.1111/j.1525-1314.1993.tb00146.x.

Hill, E.J., Baldwin, S.L. & Lister, G.S. (1992). Unroofing of active metamorphic core complexes in the D'Entrecasteaux Islands, Papua New Guinea. *Geology* **20**, 907–910, doi: 10.1130/0091-7613(1992) 020<0907:UOAMCC> 2.3.CO;2.

Hill, J., Baldwin, S.L., & Lister, G.S. (1995). Magmatism as an essential driving force for formation of active metamorphic core complexes in eastern Papua New Guinea, *Journal of Geophysical Research: Solid Earth* **100(B6)**, 10441–10451, doi: 10.1029/94JB03329.

Hofmann, A.E., Valley, J.W., Watson, E.B., Cavosie, A.J., & Eiler, J.M. (2009). Sub-micron scale distributions of trace elements in zircon. *Contributions to Mineralogy and Petrology* **158(3)**, 317-335.

Holland, T.J.B. (1980). The reaction albite= jadeite+ quartz determined experimentally in the range 600-1200 degrees C. *American Mineralogist* **65(1-2)**, 129–134.

Hwang, S.L., Shen, P., Chu, H.T., Yui, T.F., & Lin, C.C. (2001). Genesis of microdiamonds from melt and associated multiphase inclusions in garnet of ultrahigh-pressure gneiss from Erzgebirge, Germany. *Earth and Planetary Science Letters* ***188*****(1-2)**, 9-15.

Kaneko, Y., Katayama, I., Yamamoto, H., Misawa, K., Ishikawa, M., Rehman, H.U., Kausar, A.B. & Shiraishi, K. (2003). Timing of Himalayan ultrahigh-pressure metamorphism: Sinking rate and subduction angle of the Indian continental crust beneath Asia. *Journal of Metamorphic Geology* **21(6)**, 589–599.

Kington, J.D. & Goodliffe, A.M. (2008). Plate motions and continental extension at the rifting to spreading transition in Woodlark Basin, Papua New Guinea: Can oceanic plate kinematics be extended into continental rifts? *Tectonophysics* **458**, 82–95.

Kohn, M.J., Corrie, S.L., & Markley, C. (2015). The fall and rise of metamorphic zircon. *American Mineralogist* **100(4)**, 897-908.

Kooijman, E., Smit, M.A., Mezger, K., & Berndt, J. (2012). Trace element systematics in granulite facies rutile: implications for Zr geothermometry and provenance studies. *Journal of Metamorphic Geolgoy* **30(4)**, 397–412.

Korchinski, M.S., Vry, J., Little, T.A., Millet, M.A., Bicknell, R., Smith, E. & Handt, A. (2014). Timing of UHP exhumation and rock fabric development in gneiss domes containing the world's youngest eclogite Facies rocks, southeastern Papua New Guinea. *Journal of Metamorphic Geology* **32(9)**, 1019–1039.

Korsakov, A. V., & Hermann, J. (2006). Silicate and carbonate melt inclusions associated with diamonds in deeply subducted carbonate rocks. *Earth and Planetary Science Letters* **241(1-2)**, 104-118.

Kotkova J. & Harley., S.L. (2010). Anatexis during high-pressure crustal metamorphism: evidence from garnet–whole-rock REE relationships and zircon–rutile Ti–Zr thermometry in leucogranulites from the Bohemian Massif. *Journal of Petrology* **51**, 1967–2001.

Kylander-Clark, A.R.C., Hacker, B.R., Johnson, C.M., Beard, B.L., Mahlen, N.J. & Lapen, T.J. (2007). Coupled Lu–Hf and Sm–Nd geochronology constrains prograde and exhumation histories of high- and ultrahigh-pressure eclogites from western Norway. *Chemical Geology* **242(1–2)**, 137–154, http://dx.doi.org/10.1016/j.chemgeo.2007.03.006.

Kylander-Clark, A.R.C., Hacker, B.R., Johnson, C.M., Beard, B.L. & Mahlen, N.J. (2009). Slow subduction and rapid exhumation of a thick ultrahigh-pressure terrane. *Tectonics* **28(2)**, TC2003, http://dx.doi.org/10.1029/2007TC002251.

Kylander-Clark, A.R.C., Hacker, B.R. & Mattinson, C.G. (2012), Size and exhumation rate of ultrahigh-pressure terranes linked to orogenic stage. *Earth and Planetary Science Letters* **321–322**, 115–120, http://dx.doi.org/10.1016/j.epsl.2011.12.036.

Kylander-Clark, A.R.C., Hacker, B.R. & Cottle, J.M. (2013). Laser-ablation split-stream ICP petrochronology. *Chemical Geology* **345**, 99–112, http://dx.doi.org/10.1016/j.chemgeo.-2013.02.019.

Labrousse, L., Jolivet, L., Agard, P., Hébert, R., & Andersen, T.B. (2002). Crustal-scale boudinage and migmatization of gneiss during their exhumation in the UHP province of western Norway. *Terra Nova* **14(4)**, 263-270.

Labrousse, L., Prouteau, G. & Ganzhorn, A.C. (2011). Continental exhumation triggered by partial melting at ultrahigh pressure. *Geology* **39**, 1171–1174, doi: 10.1130/G32316.1.

Lang, H.J. & Gilotti, J.A. (2007). Partial melting of metapelites at ultrahigh-pressure conditions, Greenland Caledonides. *Journal of Metamorphic Geology* **25**, 129–147, doi: 10.1111/j.1525-1314.2006.00687.x.

Lapen, T.J., Johnson, C.M., Baumgartner, L.P., Mahlen, N.J., Beard, B.L. & Amato, J.M. (2003). Burial rates during prograde metamorphism of an ultra-high-pressure terrane: an example from Lago di Cignana, western Alps, Italy. *Earth and Planetary Science Letters* **215**, 57–72.

Li, Z.H., Xu, Z.Q. & Gerya, T.V. (2011). Flat versus steep subduction: Contrasting modes for the formation and exhumation of high to ultrahigh-pressure rocks in continental collision zones. *Earth and Planetary Science Letters* **301**, 65–77, doi:10.1016/j.epsl.2010.10.014.

Liou, J.G., Tsujimori, T., Zhang, R.Y., Katayama, I. & Maruyama, S., (2004). Global UHP metamorphism and continent subduction/collision. The Himalayan model. *International Geology Review* **46**, 1–27.

Little, T.A., Baldwin, S.L., Fitzgerald, P.G. & Monteleone, B. (2007). Continental rifting and metamorphic core complex formation ahead of the Woodlark Spreading Ridge, D'Entrecasteaux Islands, Papua New Guinea. *Tectonics* **26**, TC1002, doi:10.1029/2005TC001911.

Little, T.A., Hacker, B.R., Gordon, S.M., Baldwin, S.L., Fitzgerald, P.G., Ellis, S. & Korchinski, M. (2011). Diapiric exhumation of Earth's youngest (UHP) eclogites in the gneiss domes of the D'Entrecasteaux Islands, Papua New Guinea. *Tectonophysics* **510**, 39–68, doi: 10.1016/j.tecto.2011.06.006.

Little, T.A., Hacker, B.R., Brownlee, S.J. & Seward G. (2013). Microstructures and quartz lattice-preferred orientations in the eclogite-bearing migmatitic gneisses of the D'Entrecasteaux Islands, Papua New Guinea. *Geochemistry, Geophysics, Geosystems* **14(6)**, 2030–2062, doi: 10.1002/ggge.20132.

Liu F., Xu, Z., Liou, J.G., Dong, H. & Xue, H. (2007), Ultrahigh-pressure mineral assemblages in zircons from surface to 5158 m depth in cores of the main drill hole, Chinese Continental Scientific Drilling Project, southwestern Sulu belt, China. *International Geological Review* **49**: 454-478.

Liu, Q., Jin, Z.M., & Zhang, J.F. (2009). An experimental study of dehydration melting of phengite-bearing eclogite at 1.5-3.0 GPa. *Chinese Science Bulletin* **54**, 2090–2100.

Lus, W.Y., McDougall, I. & Davies, H.L. (2004). Age of metamorphic sole of the Papuan Ultramafic Belt ophiolite, Papua New Guinea. *Tectonophysics **392***, 85–101, doi: 10.1016/j.tecto.2004.04.009.

Luvizotto, G.L. & Zack, T. (2009). Nb and Zr behavior in rutile during high-grade metamorphism and retrogression: an example from the Ivrea-Verbano Zone. *Chemcial Geology* **261(3–4)**, 303–317.

Massonne, H.J., Kennedy, A., Nasdala, L. & Theye, T. (2007). Dating of zircon and monazite from diamondiferous quartzofeldspathic rocks of the Saxonian Erzgebirge-hints at burial and exhumation velocities. *Mineralogical Magazine* **71**, 407–425.

Mattinson, J.M. (2005). Zircon U-Pb chemical abrasion (“CA-TIMS”) method: combined annealing and multi-step partial dissolution analysis for improved precision and accuracy of zircon ages. *Chemical Geology* **220**, 47–66, doi: 10.1016/j.chemgeo.2005.03.011.

Mattinson, C.G., Wooden, J.L., Liou, J.G., Bird, D.K. & Wu, C.L. (2006). Age and duration of eclogite-facies metamorphism, North Qaidam HP/UHP terrane, Western China. *American Journal of Science* **306**, 683–711, http://dx.doi.org/10.2475/09.2006.01.

McDonough, W.F. & Sun, S.S. (1995). The composition of the Earth. *Chemical geology*, **120(3-4)**, 223-253.

McLean, N.M., Bowring, J.F., & Bowring, S.A. (2011). An algorithm for U-Pb isotope dilution data reduction and uncertainty propagation. *Geochemistry, Geophysics, Geosystems*, **12(6)**.

McLean, N.M., Condon, D.J., Schoene, B. & Bowring, S.A. (2015), Evaluating uncertainties in the calibration of isotopic reference materials and multi-element isotopic tracers (EARTHTIME Tracer Calibration Part II). *Geochimica et Cosmochimica Acta* **164**, 481-501, doi:10.1016/j.gca.2015.02.040.

Monteleone, B.D., Baldwin, S.L., Webb, L.E., Fitzgerald, P.G., Grove, M. & Schmitt, A.K. (2007). Late Miocene–Pliocene eclogite facies metamorphism, D’Entrecasteaux Islands, SE Papua New Guinea. *Journal of Metamorphic Geology* **25**, 245–265, doi: 10.1111/j.1525-1314.2006.00685.x.

O'Brien, P.J. (2001). Subduction followed by collision: Alpine and Himalayan examples. *Physics of the Earth and Planetary Interiors* **127**, 277–291.

Parrish, R.R., Gough, S.J., Searle, M.P. & Waters, D.J. (2006). Plate velocity exhumation of ultrahigh-pressure eclogites in the Pakistan Himalaya. *Geology* **34**, 989–992.

Proyer, A., Dachs, E. & McCammon, C. (2004). Pitfalls in geothermobarometry of eclogites: Fe^{3+} and changes in the mineral chemistry of omphacite at ultrahigh pressures. *Contributions to Mineralogy and Petrology* **147**, 305–318.

Ragozin, A.L., Liou, J.G., Shatsky, V.S. & Sobolev, N.V. (2009), The timing of the retrograde partial melting in the Kumdy-Kol region (Kokchetav Massif, Northern Kazakhstan). *Lithos* **109**, 274–284, doi:10.1016/j.lithos.2008.06.017.

Rogerson, R., Hilyard, D.B., Finlayson, E.J., Holland, D.J., Nion, S.T.S., Sumarang, R.M., Dugaman, J. & and C.D.C. Loxton, C.D.C. (1987). The geology and mineral resources of the Sepik headwaters region, Papua New Guinea, *Papua New Guinea Geological Surveys Memoir, 12*.

Rubatto, D. (2002). Zircon trace element geochemistry: distribution coefficients and the link between U-Pb ages and metamorphism. *Chemical Geology* **184**, 123–138, doi: 10.1016/S0009-2541(01)00355-2.

Rubatto, D. (2017). Zircon: The Metamorphic Mineral. *Reviews in Mineralogy and Geochemistry* **83(1)**, 261–295, https://doi.org/10.2138/rmg.2017.83.9

Rubatto, D. & Hermann, J. (2001). Exhumation as fast as subduction? *Geology* **29***,* 3–6, doi: 10.1130/0091-7613(2001) 029<0003:EAFAS> 2.0.CO;2.

Rubatto, D. & Hermann, J. (2003). Zircon formation during fluid circulation in eclogites (Monviso, Western Alps): Implications for Zr and Hf budget in subduction zones. *Geochimica et Cosmochimica Acta* **67**, 2173–2187, http://dx.doi.org/10.1016/S0016-7037(02)01321-2.

Rubatto, D. & Hermann, J. (2007a). Zircon behaviour in deeply subducted rocks. *Elements* **3**, 31–35, http://dx.doi.org/10.2113/gselements.3.1.31.

Rubatto, D. & Hermann, J. (2007b). Experimental zircon/melt and zircon/garnet trace element partitioning and implications for the geochronology of crustal rocks. *Chemical Geology* **241**, 38–61, http://dx.doi.org/10.1016/j.chemgeo.2007.01.027.

Schoene, B., Latkoczy, C., Schaltegegger, U. & Günther, D. (2010). A new method integrating high-precision U–Pb geochronology with zircon trace-element analysis (U–Pb TIMS-TEA). *Geochimica et Cosmochimica Acta* **74**, 7144–7159, doi: 10.1016/j.gca.2010.09.016.

Schmidt, M. W. & Thompson, A. B. (1996). Epidote in calc-alkaline magmas: An experimental study of stability, phase relationships, and the role of epidote in magmatic evolution. *American Mineralogist* **81 (3-4)**, 462-474, doi:10.2138/am-1996-2-420.

Sizova, E., Gerya, T. & Brown, M. (2012). Exhumation mechanism of ultrahigh pressure crustal rocks during collision of spontaneously moving plates. *Journal of Metamorphic Geology* **30**, 927–955, doi:10.1111/j.1525-1314.2012.01004.x.

Skjerlie, K.P. & Patino Douce, A.E., (2002). The fluid-absent partial melting of a zoisite-bearing quartz eclogite from 1.0 to 3.2 GPa: implication for melting in thickened continental crust and for subduction-zone processes. *Journal of Petrology* **43**, 291–314.

Smith, D.C. (1984). Coesite in clinopyroxene in the Caledonides and its implications for geodynamics. *Nature* **310**, 641–644, doi:10.1038/310641a0.

Sobolev, N.V. & Shatsky, V.S. (1990). Diamond inclusions in garnets from metamorphic rocks; a new environment of diamond formation. *Nature* **343**, 742–746, doi:10.1038/343742a0.

Spandler, C., Mavrogenes, J., & Hermann, J. (2007). Experimental constraints on element mobility from subducted sediments using high-P synthetic fluid/melt inclusions. *Chemical Geology* **239(3-4)**, 228-249.

Spear, F.S., Wark, D.A., Cheney, J.T., Schumacher, J.C., & Watson, E.B. (2006). Zr-in-rutile thermometry in blueschists from Sifnos, Greece. *Contributions to Mineralogy and Petrology* **152(3)**, 375-385.

Stepanov, A., Rubatto, D., Hermann, J., & Korsakov, A.V. (2016a). Constrasting *P–T* paths within the Barchi-Kol UHP terrain (Kokchetav Complex): Implications for subduction and exhumation of continental crust. *American Mineralogist* **101**, 788.

Stepanov, A., Hermann, J., Rubatto, D., Korsakov, A.V., & Danyushevsky, L.V. (2016b). Melting history of an ultrahigh-pressure paragneiss revealed by multiphase solid inclusions in garnet, Kokchetav massif, Kazakhstan. *Journal of Petrology* **57**, 1531–1554.

Stöckhert, B., Duyster, J., Trepmann, C., & Massonne, H.J. (2001). Microdiamond daughter crystals precipitated from supercritical COH+ silicate fluids included in garnet, Erzgebirge, Germany. *Geology* **29(5)**, 391-394.

Stöckhert, B., Trepmann, C.A., & Massonne, H.J. (2009). Decrepitated UHP fluid inclusions: about diverse phase assemblages and extreme decompression rates (Erzgebirge, Germany). *Journal of Metamorphic Geology* **27(9)**, 673-684.

Tailby, N.D., Walker, A.M., Berry, A.J., Hermann, J., Evans, K.A., Mavrogenes, J.A., O'Neil, H.St.C., Rodina, I.S., Soldatov, A.V., Rubatto, D., & Sutton, S.R. (2011). Ti site occupancy in zircon. *Geochimica et Cosmochimica Acta* 7**5(3)**, 905-921.

Taylor, B. & Huchon, P. (2002). *Active continental extension in the western Woodlark Basin: a synthesis of Leg 180 results*. in Proceedings of the Ocean Drilling Program, Scientific Results [CD ROM], vol. 180, edited by P. Huchon, B. Taylor, and A. Klaus, pp. 1–36, Ocean Drill. Prog., Texas A&M Univ., College Station, Tex.

Taylor, B., Goodliffe, A.M. & Martinez, F. (1999). How Continents break-up: insights from Papua New Guinea. *Journal of Geophysical Research: Solid Earth* **104**, 7497–7512, doi: 10.1029/1998JB900115.

Thomas, J.B., Watson, E.B., Spear, F.S., Shemella, P.T., Nayak, S.K., & Lanzirotti, A. (2010). TitaniQ under pressure: the effect of pressure and temperature on the solubility of Ti in quartz. *Contributions to Mineralogy and Petrology* **160(5)**, 743–759.

Timms, N.E., Kinny, P.D., Reddy, S.M., Evans, K., Clark, C., & Healy, D. (2011). Relationship among titanium, rare earth elements, U–Pb ages and deformation microstructures in zircon: Implications for Ti-in-zircon thermometry. *Chemical Geology* **280**, 33–46.

Tomkins, H.S., Powell, R., Ellis, D.J. (2007). The pressure dependence of the zirconium-in-rutile thermometer. *Journal of Metamorphic Geology* **25(6)**,703–713.

Tregoning, P., Lambeck, K., Stoltz, A., Morgan, P., McClusky, S.C., van der Beek, P., McQueen, H., Jackson, R.J., Little, R.P., Laing, A. & and B. Murphy, B. (1998). Estimation of current plate motions in Papua New Guinea from Global Positioning System observations. *Journal of Geophysical Research: Solid Earth* **103**, 12,181–12,203, doi: 10.1029/97JB03676.

Van Ufford, Q.A. & Cloos, M. (2005). Cenozoic tectonics of New Guinea. *American Association of Petroleum Geology Bulletin* **89**, 119–140, doi:10.1306/08300403073.

Waggoner, A., Baldwin, S.L., Webb, L.A., Little, T.A. & Fitzgerald, P.G. (2008). Temporal constraints on continental rifting and the exhumation of the youngest known UHP metamorphic rocks, SE Papua New Guinea. *Eos Trans. AGU* **89(53)**, Fall Meet. Suppl., Abstract T41B-1961.

Wallace, L.M., Stevens, C., Silver, E., McCaffrey, R., Loratung, W., Hasiata, S., Stanaway, R., Curley, R., Rosa, R. & Taugaloidi, J. (2004). GPS and seismological constraints on active tectonics and arc-continent collision in Papua New Guinea: implications for mechanics of microplate rotations in a plate boundary zone. *Journal of Geophysical Research: Solid Earth* **109**, doi:10.1029/2003JB002481.

Wallace, L.M., Ellis, S., Little, T.A., Tregoning, P., Palmer, N., Rosa, R., Stanaway, R., Oa, J., Nidkombu, E. & J. Kwazi, J. (2014). Continental breakup and UHP rock exhumation in action: GPS results from the Woodlark Rift, Papua New Guinea. *Geochemistry, Geophysics, Geosystems* **15**, 4267–4290, doi:10.1002/2014GC005458.

Wallis, S., Tsuboi, M., Suzuki, K., Fanning, M., Jiang, L., & Tanaka, T. (2005). Role of partial melting in the evolution of the Sulu (eastern China) ultrahigh-pressure terrane. *Geology* **33(2)**, 129-132.

Warren, C.J., Beaumont, C. & Jamieson, R.A. (2008). Modelling tectonic styles and ultra-high pressure (UHP) rock exhumation during the transition from oceanic subduction to continental collision. *Earth and Planetary Science Letters* **267(1-2)**, 129-145.

Watson, E.B., Wark, D.A., & Thomas, J.B. (2006). Crystallization thermometers for zircon and rutile. *Contributions to Mineralogy and Petrology* **151(4)**, 413–433.

Webb, L.E., Baldwin, S.L., Little, T.A., & Fitzgerald, P.G. (2008). Can microplate rotation drive subduction inversion?. *Geology* **36(10)**, 823-826.

Weissel, J.K., Taylor, B. & Karner, G.D. (1982). The opening of the Woodlark Basin, subduction of the Woodlark spreading system, and the evolution of northern Melanesia since mid-Pliocene time. *Tectonophysics* **87**, 253–277, doi: 10.1016/0040-1951(82)90229-3.

Whitney, D. L., & Evans, B. W. (2010). Abbreviations for names of rock-forming minerals. *American mineralogist* **95(1)**, 185-187.

Zack, T., Moraes, R., Kronz, A. (2004). Temperature dependence of Zr in rutile: empirical calibration of a rutile thermometer. *Contributions to Mineralogy and Petrology* **148(4)**, 471–48.

Zeng, L., Liang, F., Asimow, P., Chen, F., & Chen, J. (2009). Partial melting of deeply subducted continental crust and the formation of quartzofeldspathic polyphase inclusions in the Sulu UHP eclogites. *Chinese Science Bulletin* **54(15)**, 2580-2594.

Zhao, Z.F., Zheng, Y.F., Chen, R.X., Xia, Q.X., & Wu, Y.B. (2007). Element mobility in mafic and felsic ultrahigh-pressure metamorphic rocks during continental collision. *Geochimica et Cosmochimica Acta* **71**, 5244–5266.

Zheng, Y.F., Gao, X.Y., Chen, R.X., & Gao, T. (2011). Zr-in-rutile thermometry of eclogite in the Dabie orogen: Constraints on rutile growth during continental subduction-zone metamorphism. *Journal of Asian Earth Sciences* **40(2)**, 427-451.

Zirakparvar, N.A., Baldwin, S.L. & Vervoort, J.D. (2011). Lu–Hf garnet geochronology applied to plate boundary zones: Insights from the (U)HP terrane exhumed within the Woodlark Rift. *Earth and Planetary Science Letters* **309**, 56–66, doi: 10.1016/j.epsl.2011.06.016.

Zirakparvar, N.A., Baldwin, S.L. & Vervoort, J.D. (2013). The origin and geochemical evolution of the Woodlark Rift of Papua New Guinea. *Earth and Planetary Science Letters* **23**, 931–943, doi: 10.1016/j.gr.2012.06.013.

Zirakparvar, N.A., Baldwin, S.L., & Schmitt, A.K. (2014). Zircon growth in (U) HP quartzo-feldspathic host gneisses exhumed in the Woodlark Rift of Papua New Guinea. *Geochemistry, Geophysics, Geosystems*, **15(4)**, 1258-1282.

FIGURES

Fig. 1. Simplified geological map of eastern Papua New Guinea and the Woodlark Basin showing distribution of major structures and lithologies (after Baldwin et al., 2004). Box and outlined area indicate the location of the D'Entrecasteaux Islands (Fig. 2) west of the Woodlark Rift. Lower left inset shows plate-tectonic setting of the region (after Wallace et al., 2004).

Fig. 2. Simplified geological map of the D'Entrecasteaux Island gneiss domes showing major rock units, the core and carapace zones, and the dome-bounding faults, including the D'Entrecasteaux fault zone (after Davies, 1973; Hill, 1994; Little et al., 2007, 2011). Star shows the coesite locality (Baldwin et al., 2008).

Fig. 3. Backscattered electron (BSE) images showing the textural relationships in the PNG eclogites and garnet amphibolite. (a) Oiatabu Dome eclogite PNG12-95a showing amphibole and minor epidote growth that occurred at the expense of peak garnet. Omphacite and quartz are variably preserved in relation to symplectite formation; (b) Image highlighting peak assemblage of garnet, quartz, omphacite, rutile, and apatite in Oiatabu eclogite PNG12-95a; (c) Garnet surrounded by zircon with polyphase inclusions, amphibole, symplectite of plagioclase and clinopyroxene, and apatite within Mailolo Dome eclogite PNG09-041c; (d) Matrix zircon adjacent to apatite and symplecite of plagioclase and amphibole within Mailolo Dome eclogite PNG09-039b; (e) Clinopyroxene and plagioclase embayment within garnet and matrix amphibole within Goodenough Dome garnet amphibolite PNG10-035a; (f) Zircon included within matrix amphibole in Goodenough eclogite PNG12-82a; Mineral abbreviations are after Whitney & Evans (2010).

Fig. 4. Concordia diagrams of the eclogite U-Pb zircon analyses showing all LASS (grey ellipses) and/or ID-TIMS (red ellipses, Th-corrected) results for Pliocene PNG (U)HP eclogites. Insets show cathodoluminescence (CL) images with representative zircon analyzed by both ID-TIMS (red) and LASS (white) with their respective dates for 4a–d: (a) Oiatabu Dome PNG12-95a, bottom fragment of z16 was only dated by ID-TIMS, (b) Mailolo Dome PNG09-041c, (c) Mailolo Dome, PNG09-039b, and (d) Goodenough Dome PNG10-035a. (e) Goodenough Dome PNG12-82a was only dated by ID-TIMS. For the ID-TIMS analyses, the grains shown were all microsampled, and the black dashed lines denote the individual microsampled fragments. Each ellipse represents a single zircon analysis (whole grain, fragment, or single spot) and the 2σ uncertainties. Dates listed on concordia are given in Ma.

Fig. 5. Concordia diagram showing the U-Pb zircon ID-TIMS results for Oiatabu Dome host gneiss PNG12-85a, the discordant weakly deformed dikes PNG12-87b and PNG12-92b and the Goodenough Dome pegmatite PNG10-035b. Inset shows a microsampled zircon tip and corresponding ID-TIMS date from host gneiss PNG12-85a. Each ellipse represents a single zircon analysis and the 2σ uncertainties. The dates listed on concordia are in Ma.

Fig. 6. Chondrite-normalized (McDonough & Sun, 1995) zircon trace-element analyses. For each sample, results from multiple points across representative single grains are shown in addition to LA-ICP-MS analyses from all grains; Ti concentrations and the LASS U-Pb dates are shown in the CL images of representative grains. (a) Oiatabu eclogite PNG12-95a z3, (b) Mailolo eclogite PNG09-041c z13 and z21, (c) Mailolo eclogite PNG09-039b z10 and z11, (d)

Goodenough garnet amphibolite PNG10-035a z1 and eclogite PNG12-82a z8. Individual REE patterns are color-coded by the corresponding Ti concentrations (ppm). LASS spot size is ~30 microns. White scale bars are 100 microns.

Fig. 7. Representative CL images of zircon from eclogites and garnet amphibolite across the PNG domes and BSE images showing internal textures of euhedral–subhedral polyphase inclusions. Mailolo Dome eclogite zircon (PNG09-039b and PNG09-041c) contains polyphase inclusions with varying modal amounts of Ksp + Ab + Qtz and void space, whereas Oiatabu eclogite PNG12-95a zircon only preserves Ab + Qtz. Goodenough Dome garnet amphibolite contains a polyphase inclusion of Rt + Chl + Pl + Bt. Remnant gold coating is seen in cracks and edges of polyphase inclusions within zircons from PNG10-035a and PNG12-95a.

Fig. 8. Trace-element thermometry results from (U)HP eclogites and garnet amphibolite sampled across the PNG domes. Ti-in-zircon (blue diamonds) and Zr-in-rutile (red diamonds). White diamonds correspond to zircon highlighted in figure 6; the dashed line shows the range in temperatures within a single grain. Pressures given in red (see text) correspond to peak estimates used in calculating the Zr-in-rutile temperatures (Tomkins et al., 2007).

Fig. 9. Kernel density estimates for (a) Zr-in-rutile and (b) Ti-in-zircon temperatures from PNG (U)HP eclogites and garnet amphibolite. Bin size is 10 ºC for Zr-in-rutile and 15 ºC for Ti-in-zircon based on analytical uncertainty alone.

Fig. 10. Chondrite-normalized whole rock, garnet, plagioclase, and zircon trace-element data (McDonough & Sun, 1995) for PNG (U)HP eclogites. Garnet analyses in all samples show minor core to rim zoning in HREE.

Fig. 11. Left: Sketched photomicrographs (cross polar) of representative textures and mineral assemblages and associated ID-TIMS zircon ages for eclogite and garnet amphibolite from Oiatabu, Mailolo, and Goodenough Domes. Mailolo eclogite PNG08-010f is from DesOrmeau et al., 2017. Right: Cartoon *P–T* diagram showing hypothesized eclogite zircon (re)crystallization events along the exhumation path taken by the PNG UHP terrane after prograde (~7.0 Ma; Zirakparvar et al., 2011) to peak (~6.0–5.2 Ma) metamorphism (blue box; modified from DesOrmeau et al., 2017). Potential phengite breakdown reactions crossed during exhumation are shown for natural eclogites from a UHP eclogite from the Dabie Orogen (Liu et al., 2009) and a zoisite eclogite (Skjerlie & Patino Douce, 2002). Previous Mailolo and Oiatabu Domes eclogite *P–T* estimates (green stars) are from Davies & Warren (1992), Hill & Baldwin (1993), and Baldwin et al. (2004). The experimentally determined phase equilibria are from Bohlen & Boettcher (1982) for the coesite-quartz reaction and from Holland (1980) for the albite = jadeite + quartz reaction. Background facies grid from Bousquet et al. (2008). AM, amphibolite; BS, blueschist; EC, eclogite; GS, greenschist; GR, granulite. O, Oiatabu Dome; M, Mailolo Dome; G, Goodenough Dome.

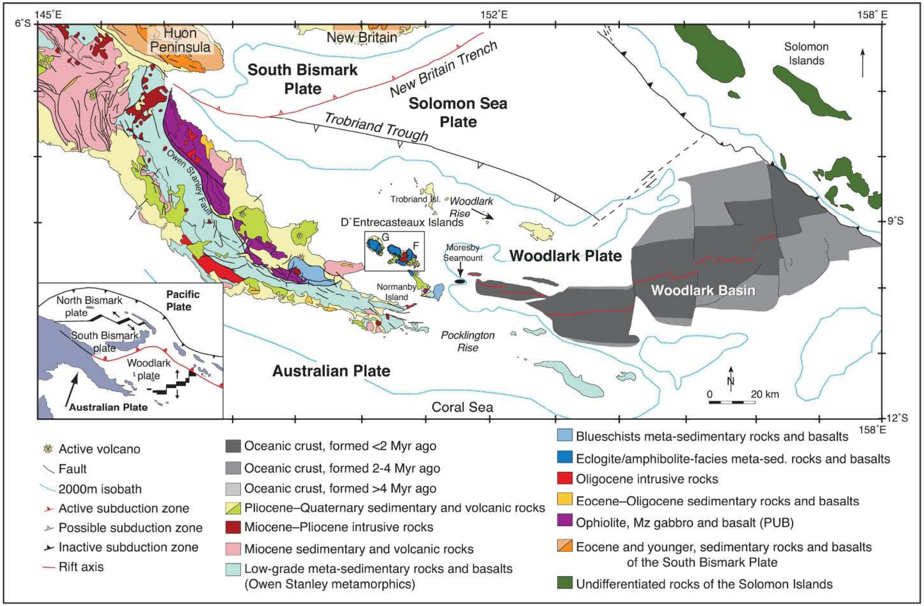

DesOrmeau et al. Figure 1

Fig. 1. Simplified geological map of eastern Papua New Guinea and the Woodlark Basin showing distribution of major structures and lithologies (after Baldwin et al., 2004). Box and outlined area indicate the location of the D’Entrecasteaux Islands (Fig. 2) west of the Woodlark Rift. Lower left inset shows plate-tectonic setting of the region (after Wallace et al., 2004).

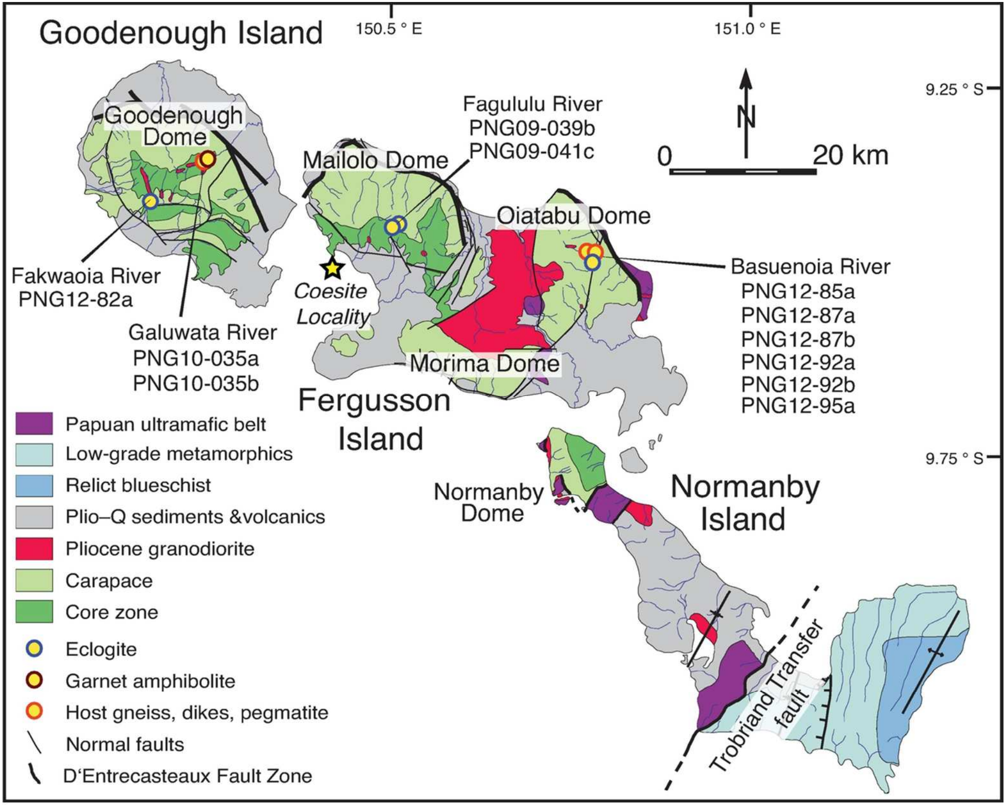

DesOrmeau et al. Figure 2

Fig. 2. Simplified geological map of the D'Entrecasteaux Island gneiss domes showing major rock units, the core and carapace zones, and the dome-bounding faults, including the D'Entrecasteaux fault zone (after Davies, 1973; Hill, 1994; Little et al., 2007, 2011). Star shows the coesite locality (Baldwin et al., 2008).

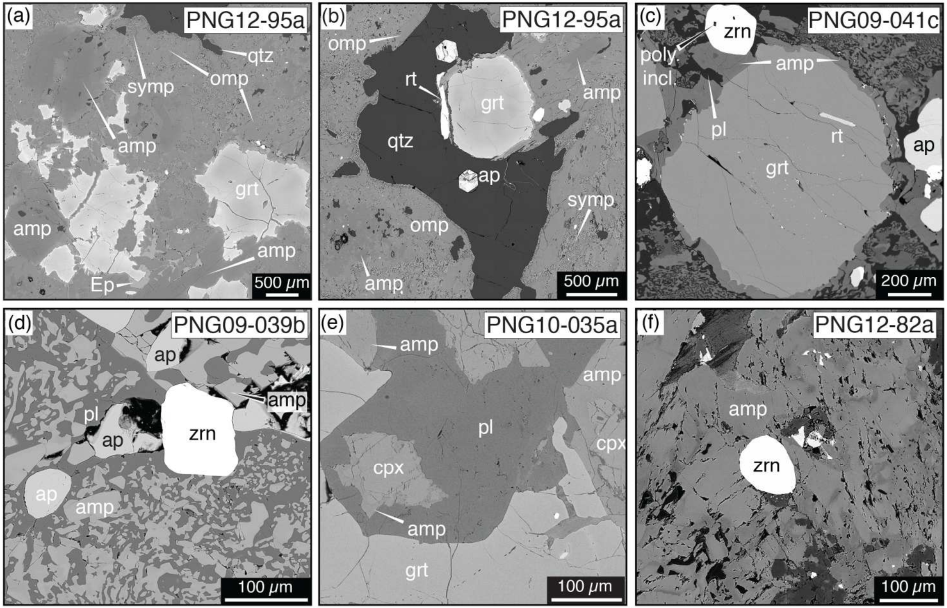

DesOrmeau et al. Figure 3

Fig. 3. Backscattered electron (BSE) images showing the textural relationships in the PNG eclogites and garnet amphibolite. (a) Oiatabu Dome eclogite PNG12-95a showing amphibole and minor epidote growth that occurred at the expense of peak garnet. Omphacite and quartz are variably preserved in relation to symplectite formation; (b) Image highlighting peak assemblage of garnet, quartz, omphacite, rutile, and apatite in Oiatabu eclogite PNG12-95a; (c) Garnet surrounded by zircon with polyphase inclusions, amphibole, symplectite of plagioclase and clinopyroxene, and apatite within Mailolo Dome eclogite PNG09-041c; (d) Matrix zircon adjacent to apatite and symplecite of plagioclase and amphibole within Mailolo Dome eclogite PNG09-039b; (e) Clinopyroxene and plagioclase embayment within garnet and matrix amphibole within Goodenough Dome garnet amphibolite PNG10-035a; (f) Zircon included within matrix amphibole in Goodenough eclogite PNG12-82a; Mineral abbreviations are after Whitney & Evans (2010).

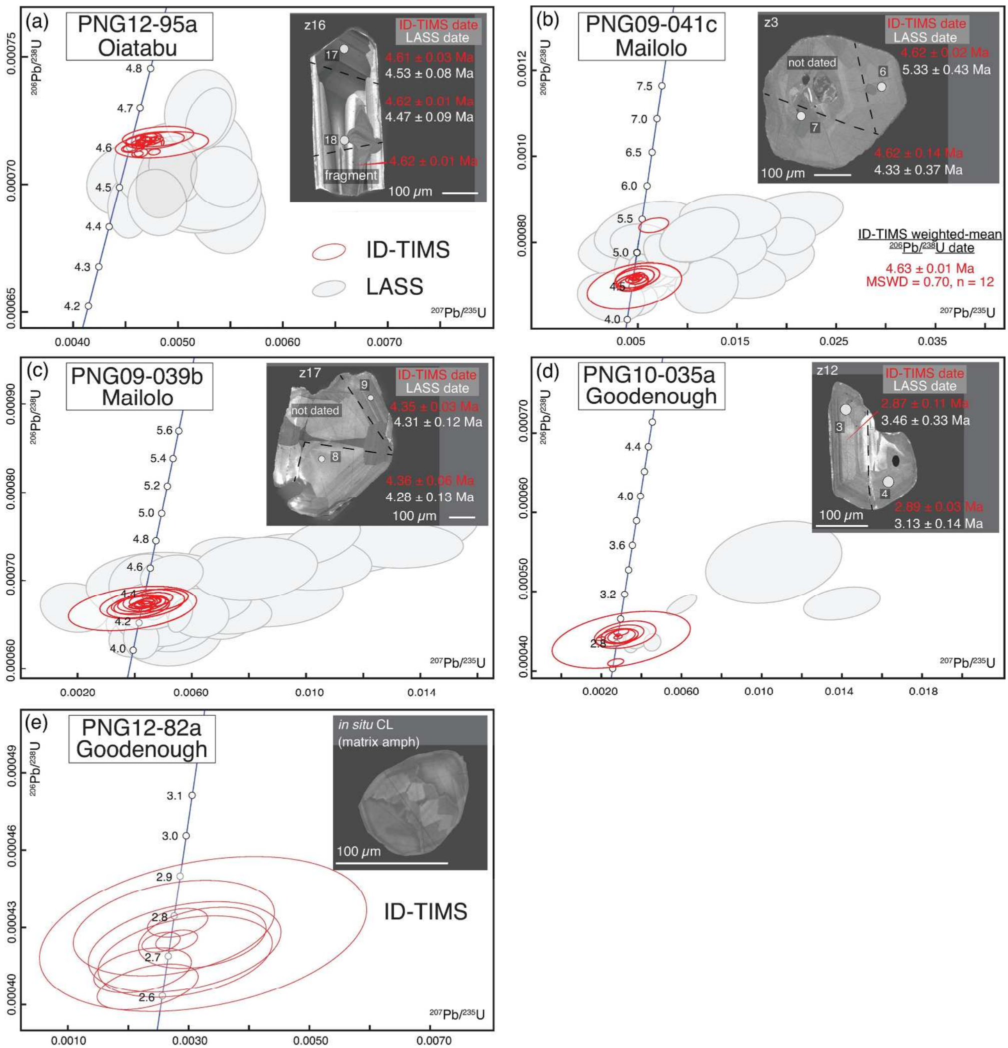

DesOrmeau et al. Figure 4

Fig. 4. Concordia diagrams of the eclogite U-Pb zircon analyses showing all LASS (grey ellipses) and/or ID-TIMS (red ellipses, Th-corrected) results for Pliocene PNG (U)HP eclogites. Insets show cathodoluminescence (CL) images with representative zircon analyzed by both ID-TIMS (red) and LASS (white) with their respective dates for 4a–d: (a) Oiatabu Dome PNG12-95a, bottom fragment of z16 was only dated by ID-TIMS, (b) Mailolo Dome PNG09-041c, (c) Mailolo Dome, PNG09-039b, and (d) Goodenough Dome PNG10-035a. (e) Goodenough Dome PNG12-82a was only dated by ID-TIMS. For the ID-TIMS analyses, the grains shown were all microsampled, and the black dashed lines denote the individual microsampled fragments. Each ellipse represents a single zircon analysis (whole grain, fragment, or single spot) and the 2σ uncertainties. Dates listed on concordia are given in Ma.

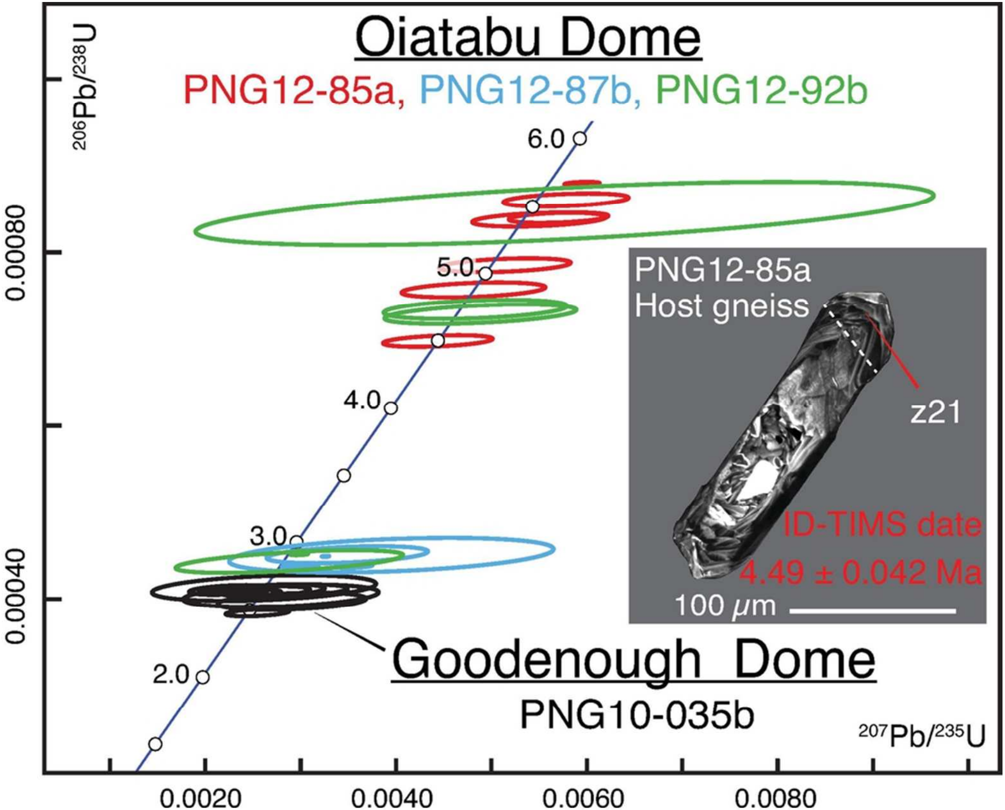

DesOrmeau et al. Figure 5

Fig. 5. Concordia diagram showing the U-Pb zircon ID-TIMS results for Oiatabu Dome host gneiss PNG12-85a, the discordant weakly deformed dikes PNG12-87b and PNG12-92b and the Goodenough Dome pegmatite PNG10-035b. Inset shows a microsampled zircon tip and corresponding ID-TIMS date from host gneiss PNG12-85a. Each ellipse represents a single zircon analysis and the 2σ uncertainties. The dates listed on concordia are in Ma.

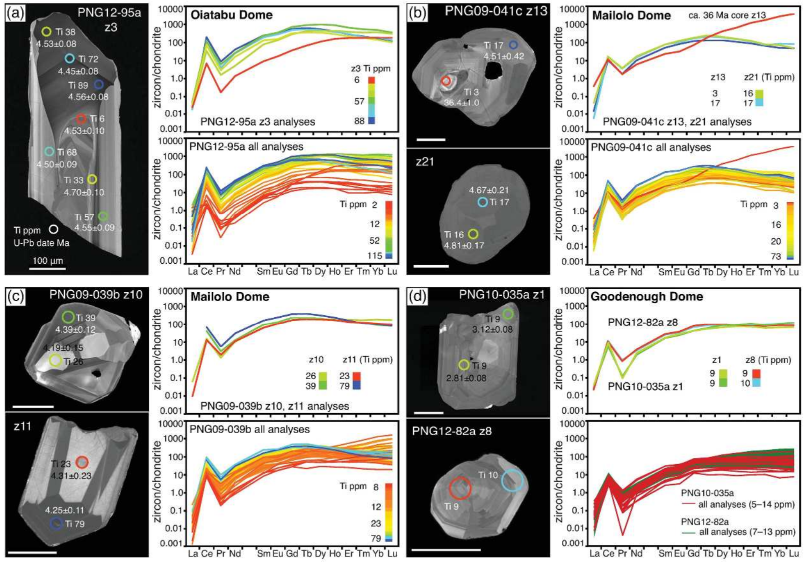

DesOrmeau et al. Figure 6

Fig. 6. Chondrite-normalized (McDonough & Sun, 1995) zircon trace-element analyses. For each sample, results from multiple points across representative single grains are shown in addition to LA-ICP-MS analyses from all grains; Ti concentrations and the LASS U-Pb dates are shown in the CL images of representative grains. (a) Oiatabu eclogite PNG12-95a z3, (b) Mailolo eclogite PNG09-041c z13 and z21, (c) Mailolo eclogite PNG09-039b z10 and z11, (d) Goodenough garnet amphibolite PNG10-035a z1 and eclogite PNG12-82a z8. Individual REE patterns are color-coded by the corresponding Ti concentrations (ppm). LASS spot size is ~30 microns. White scale bars are 100 microns.

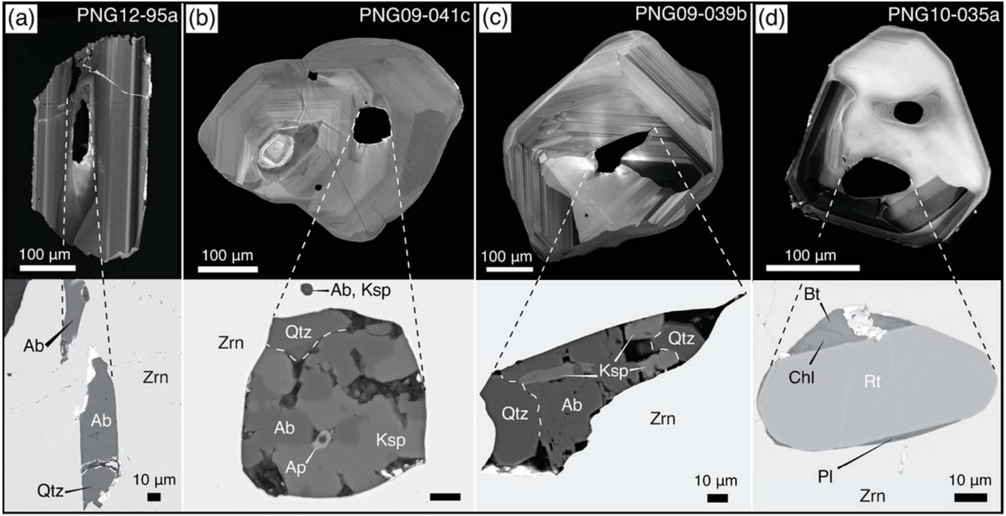

DesOrmeau et al. Figure 7

Fig. 7. Representative CL images of zircon from eclogites and garnet amphibolite across the PNG domes and BSE images showing internal textures of euhedral–subhedral polyphase inclusions. (a) Oiatabu eclogite PNG12-95a zircon only preserves Ab + Qtz, whereas (b and c) Mailolo Dome eclogite zircon (PNG09-039b and PNG09-041c) contains polyphase inclusions with varying modal amounts of Ksp + Ab + Qtz and void space. (d) Goodenough Dome garnet amphibolite contains a polyphase inclusion of Rt + Chl + Pl + Bt. Remnant gold coating is seen in cracks and edges of polyphase inclusions within zircons from PNG10-035a and PNG12-95a.

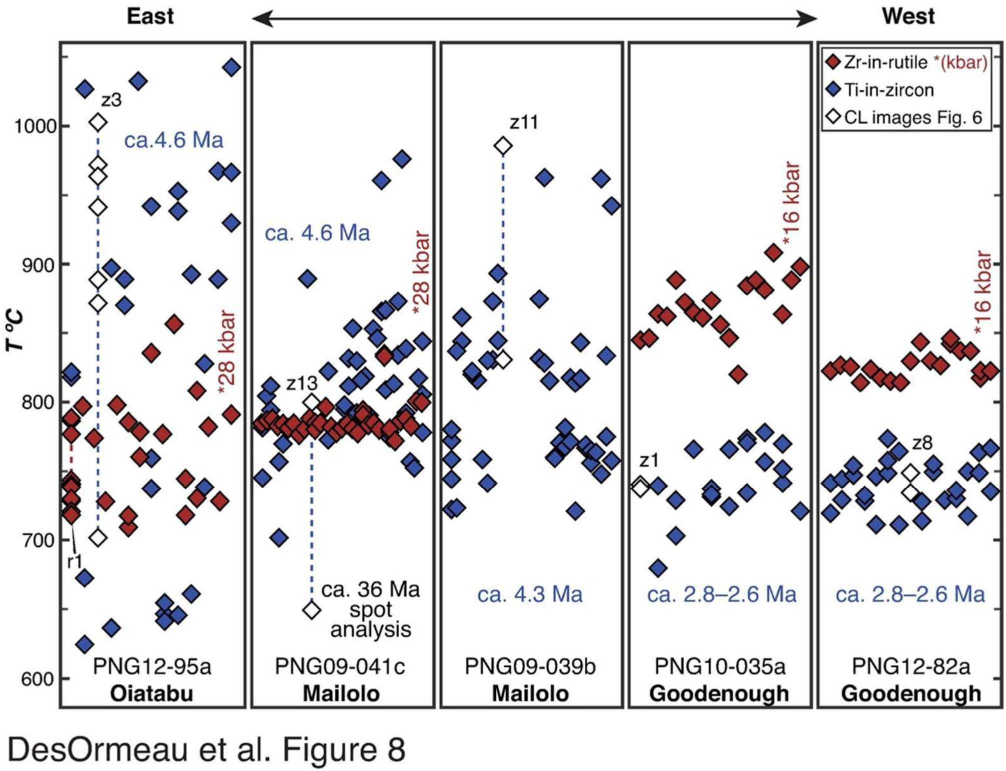

Fig. 8. Trace-element thermometry results from (U)HP eclogites and garnet amphibolite sampled across the PNG domes. Ti-in-zircon (blue diamonds) and Zr-in-rutile (red diamonds). White diamonds correspond to zircon highlighted in figure 6; the dashed line shows the range in temperatures within a single grain. Pressures given in red (see text) correspond to peak estimates used in calculating the Zr-in-rutile temperatures (Tomkins et al., 2007).

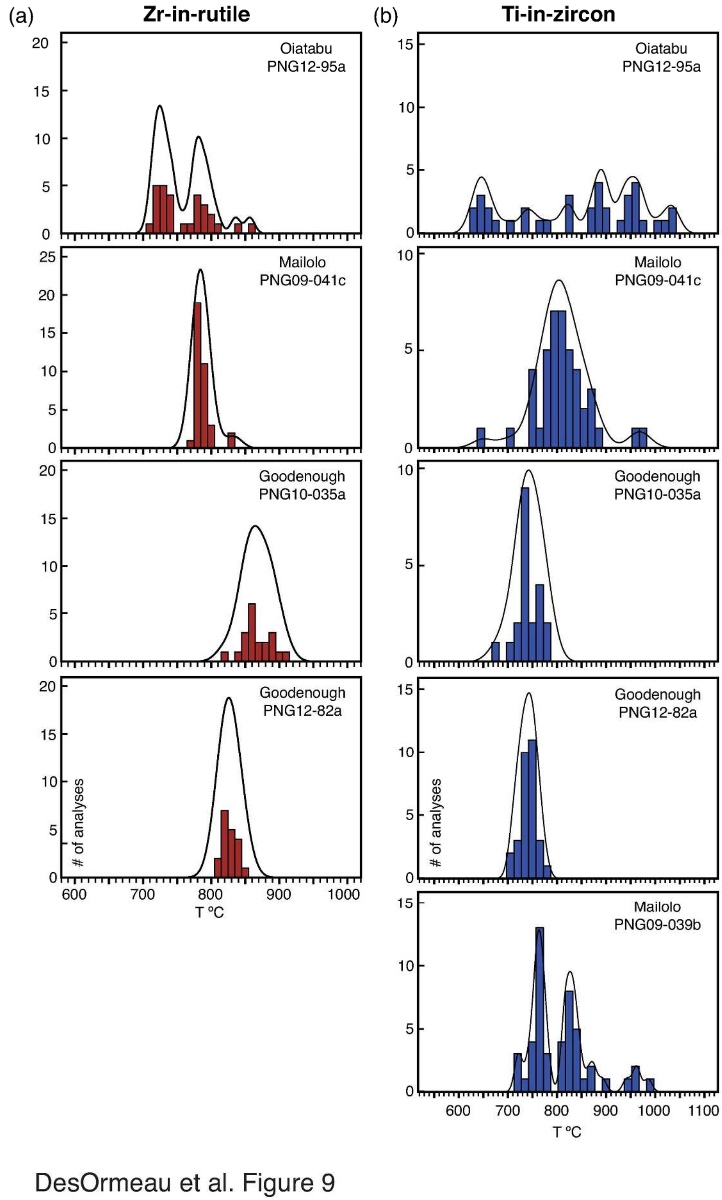

Fig. 9. Kernel density estimates for (a) Zr-in-rutile and (b) Ti-in-zircon temperatures from PNG (U)HP eclogites and garnet amphibolite. Bin size is 10 ºC for Zr-in-rutile and 15 ºC for Ti-in-zircon based on analytical uncertainty alone.

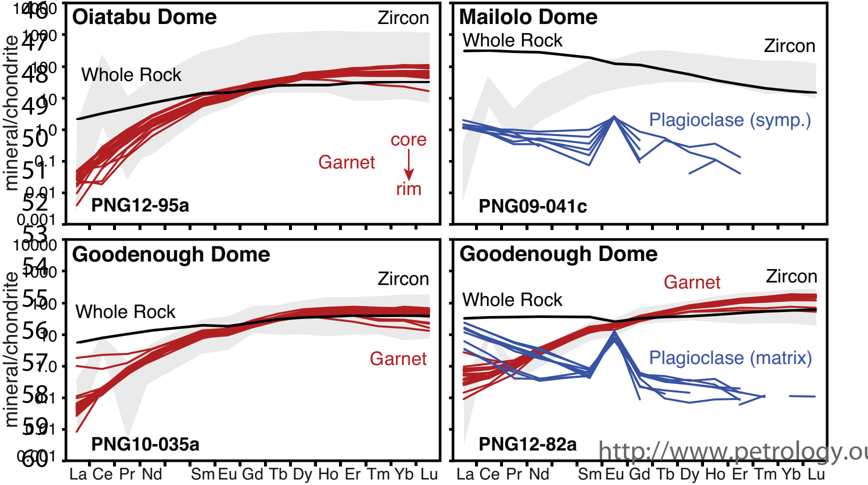
mineral/chondrite
10000
1000
100
10
1.0
0.1
0.01
0.001
Oiatabu Dome
Zircon
Whole Rock
core
Garnet
rim
PNG12-95a
Mailolo Dome
Whole Rock
Zircon
Plagioclase (symp.)
PNG09-041c
Goodenough Dome
Zircon
Whole Rock
Garnet
PNG10-035a
Goodenough Dome
Garnet
Zircon
Whole Rock
Plagioclase (matrix)
PNG12-82a
La Ce Pr Nd Sm Eu Gd Tb Dy Ho Er Tm Yb Lu
La Ce Pr Nd Sm Eu Gd Tb Dy Ho Er Tm Yb Lu

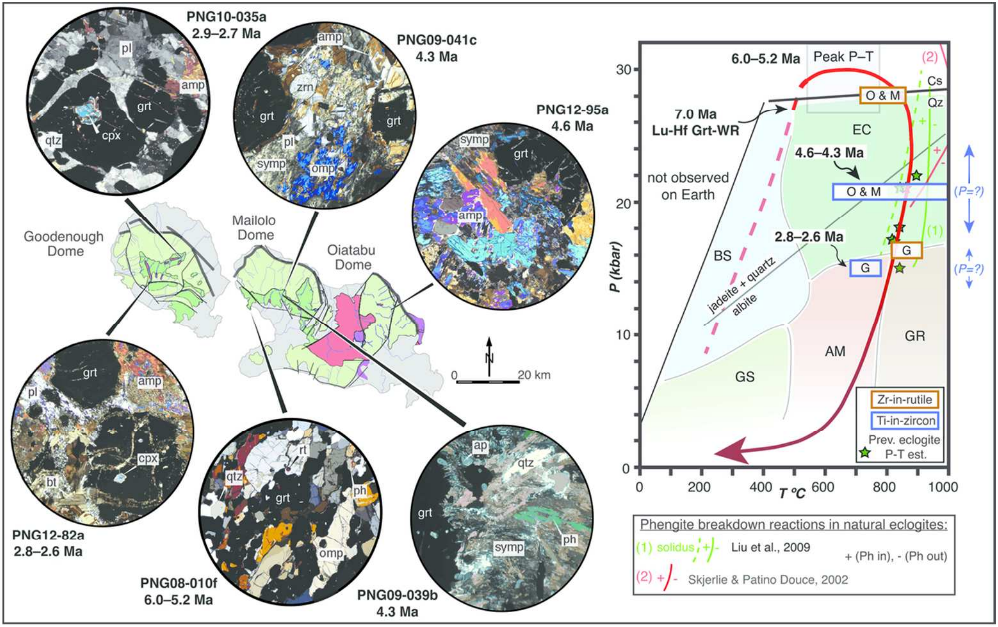

DesOrmeau et al. Figure 11

Fig. 11. Left: Sketched photomicrographs (cross polar) of representative textures and mineral assemblages and associated ID-TIMS zircon ages for eclogite and garnet amphibolite from Oiatabu, Mailolo, and Goodenough Domes. Mailolo eclogite PNG08-010f is from DesOrmeau et al. (2017). Right: Cartoon P–T diagram showing hypothesized eclogite zircon (re)crystallization events along the exhumation path taken by the PNG UHP terrane after prograde (~7.0 Ma; Zirakparvar et al., 2011) to peak (~6.0–5.2 Ma) metamorphism (blue box; modified from DesOrmeau et al., 2017). Potential phengite breakdown reactions crossed during exhumation are shown for natural eclogites from a UHP eclogite from the Dabie Orogen (Liu et al., 2009) and a zoisite eclogite (Skjerlie & Patino Douce, 2002). Previous Mailolo and Oiatabu Domes eclogite P–T estimates (green stars) are from Davies & Warren (1992), Hill & Baldwin (1993), and Baldwin et al. (2004). The experimentally determined phase equilibria are from Bohlen & Boettcher (1982) for the coesite-quartz reaction and from Holland (1980) for the albite = jadeite + quartz reaction. Background facies grid from Bousquet et al. (2008). AM, amphibolite; BS, blueschist; EC, eclogite; GS, greenschist; GR, granulite. O, Oiatabu Dome; M, Mailolo Dome; G, Goodenough Dome.